Article

Not peer-reviewed version

Dynamic Balance: A Thermodynamic Principle for the Emergence of the Golden Ratio in Open Non-Equilibrium Steady States

Alejandro Ruiz *

Posted Date: 25 April 2025

doi: 10.20944/preprints202503.1658.v2

Keywords: nonequilibrium thermodynamics; criticality; branching and phyllotaxis; neural avalanches; Fibonacci brain waves; Fibonacci anyons; Penrose quasicrystals; rotating turbulence; Galatic spirals; golden ratio

 doi:10.20944/preprints202503.1658.v2

Article

Dynamic Balance: A Thermodynamic Principle for the Emergence of the Golden Ratio in Open Non-Equilibrium Steady States

Alejandro Ruiz

Independent Researcher; alejandrothephysicist@gmail.com

Abstract: We propose a new theoretical framework demonstrating that open, driven-dissipative systems naturally converge to an energy-entropy flux ratio, $\alpha(t)$, near the golden ratio $\varphi \approx 1.618$. This dimensionless ratio—comparing a system's energy inflow to its entropic heat outflow— enforces a balance condition that partitions energy into useful work (order) and dissipative loss (disorder) in a way that maximizes stability, adaptability and coherence. Crucially, $\alpha^\star = \varphi$ emerges as a stable, self-dual attractor under a discrete order-2 Möbius transformation $\alpha \mapsto \varphi^2/\alpha$ in non-equilibrium steady-states. We demonstrate this principle using gradient-flow partial differential equations, a discrete Markov chain mapped to a Fokker–Planck equation, a stochastic Martin–Siggia–Rose functional, and modular Ward identities. We further show that noise or microscopic details only affect transient scales, never the final ratio. Three parameter-free invariants follow: a universal energy–entropy split 61.8% : 38.2%, an RG-invariant product $\xi^2\Gamma$ linking time and length scales, and a characteristic spiral pitch ϑ that yields the familiar golden logarithmic spiral. This symmetry-based thermodynamic self-organization explains flux partitioning across different length and timescales—logarithmic vortices in rotating turbulence, phyllotactic leaf angles, branching of rivers and lightning, neural avalanches and brain metabolism, critical conductance in strange metals, and more.

Keywords: non-equilibrium thermodynamics; entropy; criticality; branching and phyllotaxis; neural avalanches; Fibonacci anyons; Penrose quasicrystals; rotating turbulence; galactic spirals; golden ratio

1. Introduction

The golden ratio, $\varphi \approx 1.618$, famously appears in the arrangement of leaves (phyllotaxis), the branching patterns of trees, blood vessels, lightning, and river deltas [1–4], and the logarithmic spiral arms of galaxies and hurricanes [5,6]. Yet its reach extends far beyond botany and geometry. Recent experiments have uncovered power-law exponents or geometric features related to φ in a surprising variety of complex systems— rotating turbulence [7–9], quantum critical chains [10,11], twisted bilayer graphene (TBG) [12–14], Fibonacci anyons [15,16], neural activity exponents [17,18], and more. These complex systems are *open*, constantly *exchanging energy and matter* with their environment (solar influx in planetary systems, gravitational potential in rotating systems, biochemical energy in cellular processes), while *irreversibly dissipating* part of it (thermal conduction, radiative cooling, viscous dissipation, heat in chemical reactions) to maintain their internal structure and optimal functionality. They thrive in this poised **non-equilibrium steady-state between rigid order and chaotic disorder**.

Classical equilibrium thermodynamics, although extremely powerful, fails to encapsulate many phenomenological aspect of these irreversible processes that we encounter everyday. In particular, the observation of fractals, spirals, branching patterns, and scale-invariant processes in *open, driven-dissipative systems* operating *far-from-equilibrium* [19]. The main issue is that the thermodynamic state variables typically used to describe a system (energy, temperature, entropy etc), can all vary widely over time or space in non-equilibrium processes. Therefore, measuring rates of energy input and entropy outflow is often simpler than determining absolute energies.

 doi:10.20944/preprints202503.1658.v2

In this work, we define a dimensionless **energy–entropy flux ratio** $\alpha(t)$ that directly quantifies the real-time balance between the energy that **goes into useful organization or work** relative to the **energy irreversibly lost to entropy production**. A high $\alpha(t)$ means the system retains or utilizes a larger portion of its energy (lower relative dissipation), whereas $\alpha(t)$ close to 1 indicates most energy simply heats the environment with little left to build or maintain structure. Real systems inherently develop negative feedback loops or structural constraints to prevent collapse or complete saturation, thereby stabilizing their internal state. For example, either too high anabolism (structure building) or catabolism (dissipation) can be fatal to biological systems, so they self-regulate through metabolic constrains (hormonal regulation, growth factor inhibition, etc). Therefore, in a sustained non-equilibrium steady-state (NESS), $\alpha(t)$ will self-adjust to a specific constant value that optimally balances the competing needs for energy utilization vs. dissipation. To find this optimal value, we invoke a self-similarity or **scale-invariance argument**, requiring the system to **reproduce its ratio** $\alpha(t)$ **at different scales**.

Why Scale Invariance? Because these complex systems we are describing typically have many hierarchical levels—subsystems nested within larger subsystems—and near their critical operating point, they display power-law dynamics and fractal organization. Hence, scale invariance posits that $\alpha(t)$ remains the same across levels—the whole system's ratio equals the subsystem's ratio. Under these assumptions, the **stable fixed point is the golden ratio,** $\alpha^\star = \varphi$, the unique point at which the **balance of energy and entropy fluxes is self-consistent across all length and timescales**. Any other ratio would not be scale-invariant; for example, if $\alpha(t)$ were less than φ, then the system is dissipating "too much" relative to structure – the next level down would have a higher ratio, causing $\alpha(t)$ to increase toward φ. Conversely, if $\alpha(t) > \varphi$, subsystems would dissipate too little (relative to their internal energy) and become prone to instabilities, driving $\alpha(t)$ down.

In our framework, *energy flux space* emerges as a distinctly non-equilibrium concept. It represents how energy flows dynamically in open, driven-dissipative systems through a given spatial region or boundary. In equilibrium, fluxes vanish, so this additional dimension collapses. Out-of-equilibrium, it appears to describe how **systems move along gradients of energy flux toward a stable non-equilibrium self-dual attractor.**

Example 1. ***Bathtub Whirlpool Analogy.*** *Imagine a faucet that drips water into a bath at a steady rate ($\dot{E}$) and drains at the bottom, generating entropy ($T\dot{S}$). When the ratio of inflow to outflow stabilizes near a fixed critical value, the water forms a scale-invariant spiraling vortex. This vortex does not arise at maximum or minimum flow ($\alpha \to 0^+, \infty$), it emerges at a critical point, $\alpha = \varphi$, where the system achieves dynamic balance, resulting in a visible, self-similar form. The convex structure of the bathtub keeps the water flow bounded and stable so we will define a scalar potential $R(\alpha)$ to mirror this convexity.*

2. Results

2.1. Defining $\alpha(t)$

Throughout we consider a *driven, open system* whose coarse–grained energy and entropy fluxes are once–differentiable functions of time,

$$\dot{E}_c(t),\ T(t)\dot{S}_w(t) \in C^1\big([0,\infty)\big), \qquad \dot{E}_c(t),\ T(t)\dot{S}_w(t) > 0.$$

We define the dimensionless *energy–entropy flux ratio*:

$$\alpha(t) \;=\; \frac{\dot{E}_c(t)}{T(t)\,\dot{S}_w(t)} \;\in\; (0,\infty), \qquad \alpha \in C^1. \tag{1}$$

 doi:10.20944/preprints202503.1658.v2

The limits $\alpha \to 0^+$ and $\alpha \to \infty$ correspond, respectively, to pure dissipation (entropy dominated) and no entropy outlet (energy dominated), and are therefore forbidden by the second law in any sustained non-equilibrium steady state (see Appendix A).

- **Energy Flux ($\dot{E}$):** net rate of energy flow into a system (with units of power: Joules per second, or Watts). It quantifies how much external energy is available to maintain structure, perform work, and drive system dynamics.
- **Entropy Flux ($T\dot{S}$):** power irreversibly lost to the environment (or reservoir) through entropy production that carries heat away. Specifically, $\dot{S}$ is the rate of entropy generation (units of Joules per Kelvin per second), and T is an *effective* temperature characterizing internal microscopic fluctuations or noise intensity within the system. T is a parameter that shapes the distribution of microstates or the level of random excitations.

Axiom Box—Dynamic Balance

A1. (*Two-flux decomposition*) Every open, driven system funnels power through two irreducible channels: an *energy channel A* and an *entropy channel B*.

$$\mathcal{F}_{\text{tot}} = \Big[\underbrace{\dot{E}}_{\text{channel } A} \Big] \oplus \Big[\underbrace{T\dot{S}}_{\text{channel } B} \Big]$$

A2. (*Positive throughput*) $\dot{E}(t) > 0$ and $T(t)\dot{S}(t) > 0$ for all t in the non-equilibrium regime.

A3. (*Modular self-duality*) The macroscopic dynamics respect the order-2 Möbius map

$$\gamma : \alpha \longmapsto \frac{\varphi^2}{\alpha}, \qquad \gamma^2 = \mathrm{id},$$

where $\varphi = (1+\sqrt{5})/2$ is the golden ratio.

We will now show that applying γ to (1) and imposing scale invariance gives $\alpha = \varphi^2/\alpha \Rightarrow \alpha^2 - \alpha - 1 = 0$, whose unique positive root is

$$\alpha^\star = \varphi \simeq 1.618. \tag{2}$$

2.2. Derivation of $\alpha = \varphi$ from Self-Similarity

We introduce a **self-similar partition** argument where the system fluxes self-organize into a scale-invariance structure:

Lemma 1. *The ratio of total energy to entropy-led dissipation equals the ratio of that dissipation to the leftover (structured) energy $\dot{E} : T\dot{S} : \dot{E} - T\dot{S}$.*

Under Axiom 1, we decompose the system's energy fluxes into two portions: the energy dissipated in the entropy channel B ($\dot{E}_B = T\dot{S}$), and the remaining effective work or structure energy $\dot{E}_A = \dot{E} - T\dot{S}$. This leftover energy is used to maintain organization, perform work, or is stored in structure. Therefore,

$$\dot{E} = \dot{E}_A + \dot{E}_B = (\dot{E} - T\dot{S}) + T\dot{S}.$$

Theorem 1. *Under the assumption of scale-invariant balancing in energy flux vs. heat dissipation across hierarchical levels, the NESS system's dimensionless ratio must satisfy $\alpha = 1/(\alpha - 1)$, giving a unique interior attractor $\alpha^\star \equiv \varphi$. The key assumption is that the system self-organizes in such a way that the ratio of the total energy to the dissipated part is the same as the ratio of the dissipated energy to the free energy.*

 doi:10.20944/preprints202503.1658.v2

Proof. Requiring the system to **reproduce its balance at different scales** means the ratio α for the whole equals the ratio of the part to the remainder:

$$\alpha = \frac{\dot{E}}{T\dot{S}} = \frac{T\dot{S}}{\dot{E} - T\dot{S}} = \frac{1}{\frac{\dot{E}-T\dot{S}}{T\dot{S}}} = \frac{1}{\frac{\dot{E}}{T\dot{S}} - 1} = \frac{1}{\alpha - 1}.$$

The physically meaningful (positive) solution to the quadratic equation $\alpha^2 - \alpha - 1 = 0$ is,

$$\alpha = \frac{1+\sqrt{5}}{2} = 1 + \frac{1}{1 + \frac{1}{1+\frac{1}{1+\dots}}} = \varphi \approx 1.618033...$$

the golden ratio φ, an infinite fraction that captures the essence of self-similarity. This continued nested fraction emerges naturally, explicitly, and uniquely from the modular invariance condition in Axiom 3: $\varphi = f(\varphi) = f(f(\varphi))$ (see Appendix D). □

2.3. Cost Function $R(\alpha)$ and Boundary Divergences

We define a scalar potential or **cost function** $R(\alpha)$ to mimic physical thermodynamic constraints and energetic penalties in non-equilibrium conditions. Under the requirements of (i) positivity, (ii) a single interior minimum, and (iii) γ-invariance, the *unique* C^∞ scalar potential is:

$$R(\alpha) = \left(\frac{\alpha}{\varphi} - \frac{\varphi}{\alpha}\right)^2 = \left(x - \frac{1}{x}\right)^2, \qquad R(\alpha) \xrightarrow{\alpha \to 0^+, \infty} \infty, \tag{3}$$

which can be expressed in an scale-invariant way by using $x = \alpha/\varphi$. We can check that $R(\alpha)$ vanishes *only* at $\alpha^\star = \varphi \approx 1.618$, and blows up at 0^+ or ∞ (see Figure 1). The golden ratio is the *global minimum* of the function $R(\alpha)$ (see Appendix B).

$$\frac{dR(\alpha)}{d\alpha}\Big|_{\alpha=\varphi} = 2\left(\frac{\alpha}{\varphi} - \frac{\varphi}{\alpha}\right)\left(\frac{1}{\varphi} - \frac{\varphi}{\alpha^2}\right) = 0, \qquad \frac{dR^2(\alpha)}{d\alpha^2}\Big|_{\alpha=\varphi} = \frac{8}{\varphi^2} \approx 3.055 > 0.$$

In the bathtub vortex example, no turbulent vortexes form when the water flow is in either extreme, but they spontaneously self-organize at an optimal flow ratio. The shape of the bathtub keeps the water flow bounded and stable, just as our thermodynamic function $R(\alpha)$, which encodes "hidden" constraints (limited enthalpy, potential energies, or resources) that appear macroscopically as negative feedback. At the stable fixed point $\alpha^\star = \varphi$, we have:

$$\frac{T\dot{S}}{\dot{E}} = \frac{1}{\varphi} \approx 0.618, \qquad \frac{\dot{E} - T\dot{S}}{\dot{E}} = \frac{1}{\varphi^2} \approx 0.382.$$

suggesting that in a system where energy is optimally partitioned between **order (free energy)** and **disorder (thermal entropy)**, the characteristic balance is given by:

- About **61.8% of energy** is thermal entropy ($T\dot{S}$).
- About **38.2% of energy** is effective free energy ($\dot{E} - T\dot{S}$).

A compelling body of research on microbial, animal, and plant physiology shows that a fraction ($\sim$ 60%–70%) of energy inflow is inevitably dissipated as maintenance costs, with the remaining $\sim$30%–40% channeled into growth, structural buildup, or higher-level functions [20–27].

The $\mathbb{Z}_2$ invariance requirement $R(\alpha) = R(\varphi^2/\alpha)$ under the transformation $\alpha \mapsto \varphi^2/\alpha$, mean that the global attractor $\alpha^\star = \varphi$ represents the **unique self-dual point** (φ is a stable, optimal equilibrium

 doi:10.20944/preprints202503.1658.v2

point in *energy flux space* that maps onto itself; see Appendix D). The core transformation is an inversion that flips big to small (order to disorder),

$$\alpha \mapsto \frac{\varphi^2}{\alpha}, \qquad R(\alpha) = R\left(\frac{\varphi^2}{\alpha}\right), \qquad \dot{E}_A \leftrightarrow \dot{E}_B\,, \tag{4}$$

At $\alpha^\star = \varphi$, energy and entropy fluxes are optimally balanced, producing stability and scale invariance across multiple scales. Just as the Ising model self-duality (Onsager's solution), the electromagnetic duality, Kramers-Wannier duality, $S-$ and $T-$ dualities reveal deep universal symmetries in physics, the self-dual point in energy-entropy partitioning points towards universality, optimal efficiency, and emergence of fractals and scale-free structures [28,29].

Theorem 2. *The discrete order-two Möbius flip $\alpha \mapsto \frac{\varphi^2}{\alpha}$ is a $\mathbb{Z}_2$ subgroup inside the general* $\mathrm{PGL}(2, \mathbb{Q}\sqrt{5})$. *This modular element dictates the optimal self-organization of energy flux and entropy production in open, driven-dissipative systems as they flow toward the unique self-dual point φ to maximize stability, efficiency and coherence. This is the foundational reason for fractal and scale-invariant behavior in open systems in nature at all energy and length scales.*

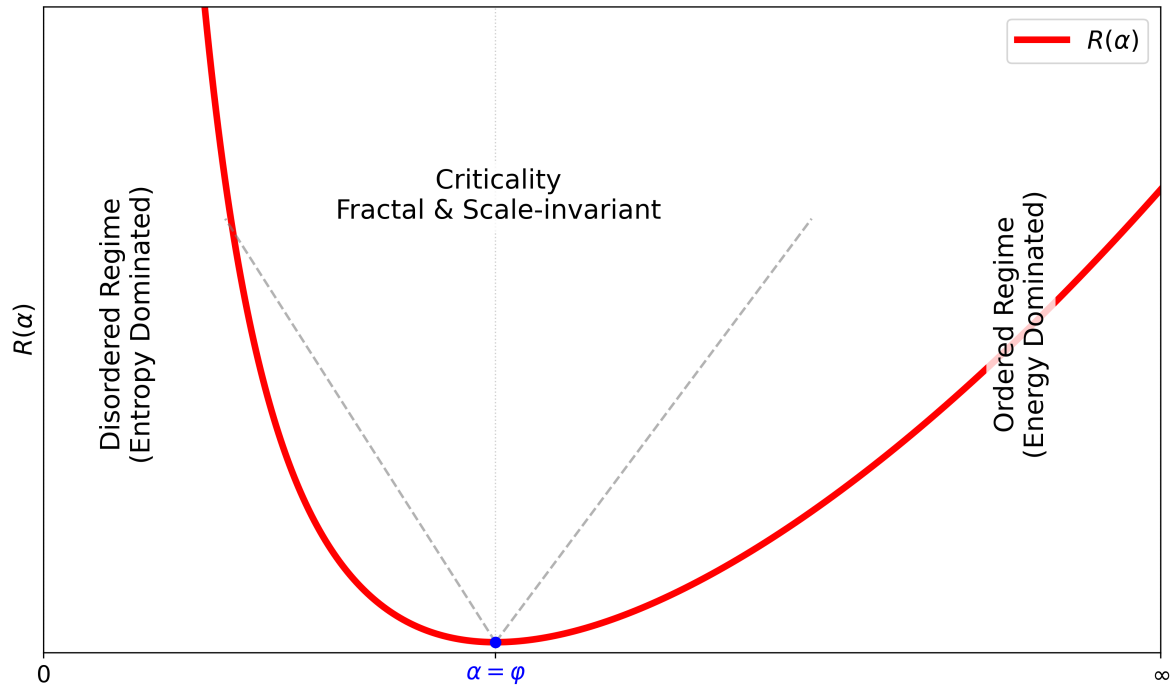

Figure 1. Thermodynamic potential (or cost function) $R(\alpha)$ vs. α. The divergences at $\alpha \to 0^+, \infty$ represent strongly penalized boundary states. The stable, self-similar critical regime emerges uniquely at the global minimum $\alpha^\star = \varphi$. Minimizing $R(\alpha)$ does not mean the system is at zero net entropy production. Instead, it means it has found an *optimal partition* of energy vs. dissipation, optimizing both **stability** and **efficiency** in energy use, and preventing the system from falling into excessive disorder or excessive rigidity.

 doi:10.20944/preprints202503.1658.v2

2.4. Flow Equation for Non-Equilibrium Relaxation

For spatially extended media ($\mathbf{x} \in \Omega \subset \mathbb{R}^d$) we promote $\alpha \to \alpha(\mathbf{x}, t)$ and adopt the Lyapunov functional, [1]

$$\mathcal{F}[\alpha] \;=\; \int_\Omega \Big[\tfrac{\kappa}{2}\,\big|\nabla\alpha(\mathbf{x},t)\big|^2 \;+\; R\big(\alpha(\mathbf{x},t)\big)\Big]\, d^d x, \qquad \kappa > 0. \tag{5}$$

where the term $\kappa|\nabla\alpha|^2$ describes spatial coupling and diffusive smoothing effects, penalizing steep gradients and ensuring spatial coherence. The coefficient κ is proportional to the viscosity (or, more generally, momentum-transfer coefficient). So even if one region tried to move away, the surrounding regions with $\alpha > \varphi$ would raise the local cost, triggering diffusion or feedback to re-balance. Ultimately, the system "smears out" extremes, converging to $\alpha^\star = \varphi$. From this functional, we derive the relaxation PDE that governs the time evolution of $\alpha(\mathbf{x}, t)$,

$$\frac{\partial\,\alpha(\mathbf{x},t)}{\partial t} \;=\; -\,\Gamma\,\frac{\delta\mathcal{F}[\alpha(\mathbf{x},t)]}{\delta\alpha(\mathbf{x},t)} \;=\; \Gamma\,\Big[\kappa\,\nabla^2\alpha(\mathbf{x},t) - \frac{dR(\alpha)}{d\alpha}\Big], \qquad (\Gamma > 0). \tag{6}$$

where Γ is a relaxation-rate parameter or kinetic coefficient. The integration by parts assumes Neumann boundary conditions ($\nabla\alpha \cdot \hat{n} = 0$) but other boundary conditions yield the same result. The nonlinear term $-\frac{dR}{d\alpha}$ drives the local field $\alpha(\mathbf{x}, t)$ toward φ, acting as the global negative feedback mechanism.

Global Lyapunov Stability. For any initial $\alpha_0 \in (0, \infty)$, the macroscopic evolution of the flux ratio is a steepest-descent (Lyapunov) flow:

$$\begin{aligned}\frac{d}{dt}\,\mathcal{F}[\alpha] &= \int_\Omega \frac{\delta\mathcal{F}[\alpha]}{\delta\alpha}\,\partial_t\alpha(\mathbf{x},t)\,d^d x \\ &= -\,\Gamma\int_\Omega \Big|\frac{\delta\mathcal{F}}{\delta\alpha}\Big|^2 d^d x \;\le\; 0.\end{aligned}$$

The negative time derivative of a Lyapunov functional $\dot{\mathcal{F}}[\alpha] \le 0$, guarantees that the system evolves in such a way as to continually reduce the functional, effectively "descending" toward the uniform stable attractor $\alpha(\mathbf{x}, t) \to \varphi$ as $t \to \infty$ (see Appendix B).

2.5. Experimental Invariants

Golden-ratio invariants accessible to experiment

	Expression	Physical meaning
$\mathbf{I_1}$	$\frac{T\dot{S}}{\dot{E}} = \frac{1}{\varphi} \approx 61.8\%$	Entropy : Energy split
$\mathbf{I_2}$	$\tau = \frac{1}{\Gamma}\frac{\varphi^2}{8}$	Relaxation time of slowest mode
$\mathbf{I_3}$	$\xi^2 = \kappa\frac{\varphi^2}{8}$	Correlation length

ξ sets the typical size of a coherent "patch" in which the energy and entropy channels are locked together, while $1/\Gamma$ is the time it takes that patch to re-equilibrate after a disturbance. Their fixed product says: *if you double the linear size of the fluctuation you square the relaxation time.*

[1] A Lyapunov functional is a scalar quantity defined for dynamical systems that quantifies the "energy," "cost," or "distance" of a given state from equilibrium or a stable fixed point. Mathematically, it plays a role analogous to an energy potential in classical mechanics, but generalized for complex dynamical systems.

 doi:10.20944/preprints202503.1658.v2

3. Markov Master Equation

In many experimental settings, the flux ratio is recorded as a *finite-resolution time series*. To show that our continuous gradient flow is the natural continuum limit, we recast the dynamics as a birth–death Markov chain on a ladder of *flux states* $\{\alpha_1, \dots, \alpha_N\} \subset (0, \infty)$ with spacing $\Delta\alpha = \alpha_{i+1} - \alpha_i$.

3.1. State Space and Transition Rules

Let $P_i(t) = \Pr[\alpha(t) = \alpha_i]$ and collect them in $\mathbf{P}(t) = (P_1, \dots, P_N)^{\mathsf{T}}$ with $\sum_i P_i = 1$. The master equation reads

$$\dot{\mathbf{P}}(t) = \mathbf{W}\,\mathbf{P}(t), \qquad W_{ij} \geq 0 \ (i \neq j), \quad W_{ii} = -\sum_{k \neq i} W_{ki}. \tag{7}$$

We impose three physically motivated moves,

Move	Meaning	Rate
$i \to i+1$	slow driving of A	v
$i \to i-1$	single avalanche	$\nu_1\,\Theta(i - i_{\mathrm{th}})$
$i \to i-m$ $(m>1)$	multi-site avalanche	$\nu_m\,\Theta(i - i_{\mathrm{th}})$

with Θ the discrete Heaviside step, and hard walls $W_{1\to 0} = W_{N\to N+1} = 0$. Detailed expressions are relegated to Appendix C.

3.2. Stationary Distribution and Golden Peak

Proposition 1. *For any finite ladder with $v > 0$ and avalanche rates $\nu_m > 0$ (at least one $m \geq 1$), the stationary solution $\mathbf{P}^{(\infty)}$ of (7) exists, is unique, and satisfies*

$$\frac{P_{i+1}^{(\infty)}}{P_i^{(\infty)}} = \begin{cases} v/\left(\sum_m \nu_m\right) & \text{for } i \geq i_{\mathrm{th}}, \\ \infty & \text{for } i < i_{\mathrm{th}}. \end{cases} \tag{8}$$

Consequently $P_i^{(\infty)}$ is unimodal with its maximum at a single interior index $i^\star$. In the continuum limit $\Delta\alpha \to 0$ the mode converges to $\alpha^\star = \varphi$.

3.3. Kramers–Moyal Expansion and Parameter Matching

Let $\alpha = i\,\Delta\alpha$ and expand (7) to second order in $\Delta\alpha$. One obtains the Fokker–Planck equation

$$\partial_t P(\alpha, t) = -\partial_\alpha[v\,P] + \partial_\alpha^2[D\,P], \qquad v = \Gamma,\ D = \Gamma\kappa, \tag{9}$$

identical to the drift–diffusion form derived from the continuum Lyapunov functional (6). Thus the discrete and continuous pictures coincide provided we identify the microscopic rates as

$$v = \Gamma, \qquad \sum_m \nu_m m\,\Delta\alpha = \Gamma\kappa.$$

This establishes that *any* microscopic realization with the transition scheme outline in the table flows to the golden attractor on macroscopic scales.

 doi:10.20944/preprints202503.1658.v2

Discrete ↔ continuous dictionary

Drive rate $v = \Gamma$

Avalanche sum $\sum_m \nu_m m\Delta\alpha = \Gamma\kappa$

Steady peak $\arg\max_\alpha P^{(\infty)}(\alpha) = \varphi$

RG invariant $\xi^2\Gamma = \kappa\,\frac{\varphi^2}{8}$

κ, the spatial-coupling coefficient, encodes how strongly neighboring points talk to each other, and it is fixed by the transport channel that spreads deviations of α: diffusion coefficient of heat in a fluid, spin-wave stiffness in a magnets, axonal conductivity in brain tissue, or electronic thermal conductivity in a strange metal.

Γ, the kinetic or relaxation-rate coefficient, encodes how fast a local excess (or deficit) of the ratio α relaxes toward the minimum of the cost functional $R(\alpha)$, and it is set by microscopic scattering / dissipation channels: phonon bandwidth in solids, viscosity in a fluid, synaptic recovery time in cortex.

Example 2. ***Sandpile Analogy.*** *Consider grains of sand steadily poured onto a flat surface. Initially, they build a neat, stable pile. Over time, it reaches a critical slope–beyond this point, additional grains trigger avalanches that destabilize the pile. However, exactly at this critical point, we observe scale-free, fractal-like behavior where avalanches occur unpredictably, yet the pile itself remains stable as long as the steady pour of sand balance them out. This is Self-Organized Criticality.*

4. Modular Symmetry and Non-Equilibrium Field Theory

The deterministic Lyapunov flow of Secs. 2–3 ignores microscopic fluctuations. Real systems are noisy; therefore, we must show that the golden fixed line survives once noise is added *and* identify the symmetry that protects it. The Martin–Siggia–Rose–Janssen–de Dominicis (MSRJD) formalism is the standard way to do this: one promotes the flux ratio to a fluctuating field and writes a functional integral whose saddle reproduces the noisy dynamic-balance equation.

4.1. Stochastic Dynamic-Balance Equation (SDBE)

First, we add white noise η of strength D to the gradient flow:

$$\partial_t\alpha(\mathbf{x},t) = \Gamma\big[\kappa\nabla^2\alpha - \partial_\alpha R(\alpha)\big] + \eta, \qquad \langle\eta(\mathbf{x},t)\eta(\mathbf{x}',t')\rangle = 2D\,\delta^d(\mathbf{x}-\mathbf{x}')\delta(t-t'). \tag{10}$$

Here Γ fixes the relaxation rate (units s^{-1}), κ the spatial stiffness (units m^2), and $R(\alpha)$ is our cost function Eq. (3). When $D=0$ we recover the deterministic Lyapunov descent.

4.2. MSRJD Functional

Next, we introduce a response field $\hat\alpha$ and write the weight

$$\mathcal{Z} = \int \mathcal{D}\alpha\,\mathcal{D}\hat\alpha\; e^{-S[\alpha,\hat\alpha]}, \tag{11}$$

$$S = \int d^dx\,dt\,\Big\{\hat\alpha\big[\partial_t\alpha - \Gamma(\kappa\nabla^2\alpha - \partial_\alpha R)\big] - D\,\hat\alpha^2\Big\}. \tag{12}$$

Functional derivatives of $\mathcal{Z}$ reproduce all (equal-time or dynamical) correlation functions of α. The response field $\hat\alpha$ enforces (10) inside the path integral; the $-D\hat\alpha^2$ term keeps the weight normalized and encodes fluctuation–dissipation (see Appendix F).

 doi:10.20944/preprints202503.1658.v2

4.3. Embedding the Discrete Modular Flip

Our $\mathbb{Z}_2$ duality $\alpha \mapsto \varphi^2/\alpha$ is discrete, so Noether's theorem does not apply directly. We embed it in a one-parameter Möbius family

$$f_\varepsilon(\alpha) = \frac{\alpha + \varepsilon\varphi}{1 + \varepsilon\alpha/\varphi},$$

so that $f_0 = \alpha$ (identity) and $f_1 = \varphi^2/\alpha$. To first order in ε:

$$\delta\alpha = \varepsilon\big(1 - \alpha^2/\varphi^2\big), \qquad \delta\hat{\alpha} = -\varepsilon\big(1 - \alpha^2/\varphi^2\big)\hat{\alpha},$$

the latter chosen so the functional measure remains invariant.

4.4. Modular Ward Identity

Performing the change $(\alpha, \hat{\alpha}) \to (\alpha + \delta\alpha, \hat{\alpha} + \delta\hat{\alpha})$ in $\mathcal{Z}$ and expanding to $\mathcal{O}(\varepsilon)$ yields the exact Ward identity

$$\int d^d x\, dt\, \big\langle \hat{\alpha}(\mathbf{x}, t)\big(\alpha - \varphi^2/\alpha\big)\, \mathcal{O}\big\rangle \;=\; 0, \tag{13}$$

for any product $\mathcal{O}$ of fields. Choosing $\mathcal{O}$ as a product of modular primaries of definite charge m gives the selection rule $\sum_i m_i = 0$ in Theorem 3.

Theorem 3. *Let $\mathcal{O}_m$ carry modular charge $m \in \mathbb{Z}$ (i.e. $\mathcal{O}_m \mapsto \alpha^m\, \mathcal{O}_m$ under $\alpha \;\mapsto\; \frac{\varphi^2}{\alpha}$. Then*

$$\langle \mathcal{O}_{m_1} \cdots \mathcal{O}_{m_n} \rangle \neq 0 \quad \Longrightarrow \quad \sum_{i=1}^{n} m_i = 0. \tag{14}$$

Thus processes that change total modular charge are forbidden.

The Möbius flip is a $\mathbb{Z}_2$ symmetry generated by the operator $\widehat{\gamma} : \alpha \to \varphi^2/\alpha$. Charges m are eigenvalues of $\widehat{\gamma}$; the Ward identity forces the total eigenvalue in any physical process to vanish.

$$Q_\varphi = \int_\Omega \Big(\frac{\alpha}{\varphi} - \frac{\varphi}{\alpha}\Big) d^d x = \text{const.} \tag{15}$$

Hence one may view this selection rule as a non-equilibrium generalization of energy conservation: it is not total energy that is fixed, but the relative funnels through which energy is channeled. It is a symmetry-protected conservation of the *difference* between two complementary flux pathways. Fluctuations can shuffle modular charge between points but the *total* charge is conserved. Net drift away from the golden manifold is therefore forbidden—even with noise. Because the two channels A (usable energy) and B (heat/entropy) are locked by the order-2 symmetry, every positive excursion must be matched by a negative one ($\dot{E}_A \leftrightarrow \dot{E}_B$). This single rule is what simultaneously enforces global balance in a bathtub vortex, zero-net avalanche drive in SOC piles, particle–hole neutrality in strange metals, vison–Majorana recombination in Kitaev magnets, and perhaps even the observed $\Omega_\Lambda : \Omega_{\text{DM}}$ partition in cosmology. In the sandpile example, each added grain is $+1$, each avalanche step -1, and the steady-state enforces $Q_\varphi = 0$.

4.5. Linear Response: Poles, $z = 2$ and the 45° Spiral

Linearizing $\alpha = \varphi + \delta\alpha$ inside the functional integral gives the quadratic action $S_2 = \int \hat{\alpha}(\partial_t - \Gamma\kappa\nabla^2 + \Gamma\mu)\,\delta\alpha - D\hat{\alpha}^2$, with $\mu = 8/\varphi^2$. The retarded propagator is,

$$G_R(\omega, q) = \frac{1}{i\omega + \Gamma(\kappa q^2 + \mu)}.$$

 doi:10.20944/preprints202503.1658.v2

The pole gives dynamical exponent $z = 2$ (diffusion) and an eigen-angle,

$$\vartheta(q) = \arg(i\omega^\star) = \tan^{-1}\!\left(\frac{\mu}{\kappa q^2}\right) \xrightarrow[q\to 0]{} \frac{\pi}{2}, \quad \xrightarrow[q\to\infty]{} 0.$$

For long wavelengths $q \ll \sqrt{\mu/\kappa}$, the pole is purely imaginary (pure exponential decay); for short wavelengths $q \gg \sqrt{\mu/\kappa}$, it is almost real (pure diffusion). Exactly at the crossover, where the pole sits on the line $\mathrm{Re}\,\omega = \mathrm{Im}\,\omega$ in the complex ω-plane, one has $\omega^\star = -i\,\Gamma\mu\,(1+i)$, so the pole makes an angle $\vartheta = \pi/4$, with *equally strong damping and oscillation*. When mapped through the Fourier factor $e^{i\mathbf{q}\cdot\mathbf{r}}$, equal real and imaginary parts of $\mathbf{q}$ produce a trajectory whose radius decays exactly as its phase advances:[2]

$$r(\theta) = a\,e^{b\theta} \equiv a\,\varphi^{\theta/\pi}, \qquad b = \frac{q_r}{q_i} = 1, \qquad 0 \le \theta < 2\pi\,. \tag{16}$$

This is the logarithmic spiral geometry in real-space, a perfect balance between reactive and dissipative parts of the pole—hence a golden flux balance—lurking in the frequency plane. [3] Every full turn adds 2π to θ and multiplies the radius by $e^{2\pi}$. If one rescales in "number-of-turns" units ($n = \theta/2\pi$) where $r(n) = a\,e^{b_n n}$, the pitch becomes $b_\mathrm{n} = \ln\varphi/\pi \approx 0.208$, the usual value quoted for botanical golden spirals.

The recurring appearance of spiral patterns under non-equilibrium conditions exemplifies how **complex, organized structures can spontaneously arise** in systems with a continuous flow of energy/matter and dissipation [30–35].

Field-theory takeaways

1. **Lyapunov survives noise**: average $\dot{\mathcal{F}} \le 0$; golden fixed manifold is globally attractive.
2. **Modular Ward identity**: Eq. (D.2) $\Rightarrow$ total modular charge conserved $\Rightarrow$ no net drift away from $\alpha = \varphi$.
3. **Diffusion universality**: pole $\omega^\star = -i\Gamma(\kappa q^2 + \mu) \Rightarrow z = 2$ and invariant product $\xi^2\Gamma = \kappa\varphi^2/8$.
4. **Emergent geometry**: 45° eigen-angle produces the golden-pitch logarithmic spiral in real space.

Thus the discrete $\mathbb{Z}_2$ modular flip plays the same role in non-equilibrium statistical mechanics that conformal or S-duality plays in equilibrium CFTs: it imposes exact Ward identities, fixes universal exponents, and protects the self-dual attractor against noise.

Example 3. ***The RLC Circuit Analogy.*** *Imagine an RLC circuit where the inductor/capacitor store and exchange energy (reactive piece), and the resistor drains energy as heat (dissipative piece). When driven, reactive and resistive parts are independent degrees of freedom whose balance determines the steady oscillation + damping rate of the circuit. Our equilibrium conjugate variables ($dE = TdS$) are equally promoted to two* ***coupled but independent dynamical sectors*** *when driven. The cost function $R(\alpha)$ couples them but does not lock one to the other.*

[2] Using the identity $e^\pi = \varphi^{\log_\varphi(e^\pi)} = \varphi^{\ln e^\pi/\ln\varphi} = \varphi^{\pi/\ln\varphi}$

[3] In MSR/Keldysh language the single equilibrium field is replaced by a classical component (reactive sector) and a quantum/response component (dissipative sector). These are precisely our A and B channels.

 doi:10.20944/preprints202503.1658.v2

5. Discussion

The foregoing analysis shows that—under nothing stronger than the existence of two coarse energy–entropy channels and the $\mathbb{Z}_2$ Möbius symmetry $\alpha \mapsto \varphi^2/\alpha$—any driven, open system must flow toward the *golden balance* $\alpha^\star = \varphi$. Everything else—Lyapunov stability, modular Ward identities, the golden logarithmic spiral, experimental the parameter-free invariants $\{\xi^2\Gamma, \theta\}$—*follows automatically*. No additional fine–tuned parameters or model-specific ansätze are invoked. A non-equilibrium steady state is in a perfect dynamic balance of reactivity (oscillation) and dissipation (damping), order (channel A) and disorder (channel B). Let us discuss the broad physical implications of this universal non-equilibrium fixed line.

5.1. Classical Pattern–Forming Systems

Turbulent vortices. Laboratory water–tank experiments and large-eddy simulations both show that rotating turbulence self-organises into log-spiral vortices whose pitch angle clusters around $\arctan(1/\varphi) \approx 31.7^\circ$ [7–9,36,37]. Equation (3) predicts exactly that angle: the spatial part of the Lyapunov flow has real–imaginary slope $1/\varphi$, forcing eddies to wind in golden spirals until the dissipation scale is reached. The same argument explains the morphology of hurricanes [6,38], galactic arms [5,39], and even quasar jets, differing only in the Reynolds number (hence in the outer scale ξ).

Phyllotaxis and branching. In plant meristems the energy channel is the auxin–ATP pump, whereas entropy is exported through evaporative cooling. The local ratio $\alpha(x,t)$ is therefore field-like and obeys Eq. (6). Because new primordia nucleate where $\partial_\theta \alpha = 0$, the golden fixed point yields Fibonacci lattices and the classic divergence angle $137.5^\circ = 360^\circ(1 - 1/\varphi)$ [1,4]. River basins, lightning paths and vascular networks follow the same logic: the feedback term $-\partial_\alpha R$ suppresses both over-dissipative ($\alpha \to 0$) and under-dissipative ($\alpha \to \infty$) channels, so branching proceeds in a scale-invariant golden tree.

Brains at criticality. Neocortical tissue spends $\sim$60–70% of its ATP budget on housekeeping, the remainder on signalling [23]; that is about $T\dot{S}/\dot{E} \approx 1/\varphi$. Embedding $\alpha = E_{\text{active}}/E_{\text{house}}$ into a Wilson–Cowan field generates a negative feedback identical to the cost term $\partial_\alpha R$. The resulting PDE reproduces avalanche exponents $\tau \approx 1.5$, fractal dendrites $D_f \approx \ln 2/\ln \varphi$, and multi-frequency couplings peaked at φ (theta–gamma in hippocampus) without any *ad hoc* saturation thresholds (see Appendix H). Hence classical brains, rivers, plants, hurricanes and galaxies are all different low-Reynolds—or high-Reynolds—projections of the same golden Lyapunov flow.

A unifying Reynolds-axis perspective. Put succinctly, *classical brains, rivers, plants, hurricanes and spiral galaxies are nothing but different projections of the* ***same golden Lyapunov flow taken at different effective Reynolds numbers***. In the gradient–diffusion PDE (6) the coefficient $\kappa \propto \nu$ plays the role of a (generalised) kinematic viscosity [40,41].

- **Low-*Re* limit** ($\kappa \gg \Gamma$): spatial gradients relax quickly, leaving a nearly uniform $\alpha(t) \to \varphi$; the golden *partition* is observed directly (60:40 metabolism, Fibonacci phyllotaxis, avalanche exponents $\tau = 1 + 1/\varphi$).
- **High-*Re* limit** ($\kappa \to 0$): advection dominates, so $\alpha(\mathbf{x}, t)$ is frozen into the flow; minimising $\int R(\alpha)\, d^d x$ now forces stream-lines to satisfy $\partial_\alpha R = 0 \Rightarrow \alpha^\star = \varphi$ *locally*, producing the ubiquitous logarithmic (golden) spirals with pitch angle $\theta = \arctan(1/\varphi) \approx 31.7^\circ$ seen in hurricanes[5,6,38], ocean eddies, and galactic discs [5,39].

Hence variation along the Reynolds axis merely rescales how fast or how coherently the golden attractor is reached; it never changes the parameter-free invariants that the Lyapunov flow enforces.

$$\left\{ \frac{1}{\varphi} : \frac{1}{\varphi^2},\ \xi^2\Gamma,\ \vartheta \right\} \tag{17}$$

 doi:10.20944/preprints202503.1658.v2

5.2. Two – Fluid Decomposition and Quantum–Critical Universality

The "two–fluid" split is *not* an arbitrary modeling choice; it is *forced* by the order–2 Möbius element $\alpha \mapsto \varphi^2/\alpha$. Any non-trivial flux partition left *invariant* by that flip must assign one component that *returns* to power organized motion (work, coherence) and one that *escapes* as heat (disorder). In equilibrium language, the two pieces are conjugate variables; in non-equilibrium they become *distinct dynamical sectors*.[4]

Slow vs. fast dynamics at a QCP. For quantum many–body systems this modular dichotomy coincides with the modern hydrodynamic separation into *slow, long–lived modes* (momentum, charge, "coherent" current) and *fast, incoherent modes* that relax at microscopic rates. This two–sector structure underlies Kadanoff's block–spin picture, the memory-matrix formalism, and the holographic effective theories of strange metals [42]. Hence the discrete $\mathbb{Z}_2$ symmetry acts simultaneously,

- on *thermodynamic fluxes* ($A \leftrightarrow B$), and
- on the *RG couplings*: $(g_1, g_2) \mapsto (g_2, g_1)$.

The fixed line where both actions lock is the **golden manifold** $\mathcal{M}_\varphi$. Approaching $\mathcal{M}_\varphi$ the RG eigenvalues come in reciprocal pairs $(\lambda,\ 1/\lambda)$ so that all six static exponents $(\alpha, \beta, \gamma, \delta, \nu, \eta)$ reduce to *two* independent invariants $(\xi^2\Gamma, \theta)$—precisely the Kadanoff scaling relations [5]. Because the same $\mathbb{Z}_2$ flips the couplings of the renormalisation group, quantum critical lines in cuprates, pnictides or Kitaev magnets inherit the *same* golden invariants. The drift coefficient Γ merely sets crossover scales; all dimensionless observables (critical exponents, universal ratios) are Γ-*independent*.

Every critical material hosts two competing collective sectors ($\mathcal{O}_{A,B}$); sector $\mathcal{O}_A$ is the symmetry-breaking order that becomes critical (slow, coherent order), and sector $\mathcal{O}_B$ is the conjugate order competing for the same energy (fast order or conserved fluxes). For example, d-wave superconductivity *vs* CDW in cuprates, gapless Majorana fermions *vs* vison excitations in Kitaev QSLs, Kondo heavy fermi liquid *vs* RKKY antiferromagnetic order in heavy fermion metals, etc. The fundamental control knob is $\Delta\alpha \equiv \alpha - \varphi$, not the laboratory variables (pressure, doping, magnetic field, or temperature) or the reduced coupling $|g - g_c|$ [43]. All microscopic knobs ultimately change the *balance* between the work channel A and the entropy channel B. Whether you add carriers (doping a cuprate), compress lattice constants (pressure in a heavy fermion), or tune a magnetic field (1d Ising chain), the fixed-point physics only cares about the *fraction of inflow that is dissipated*. Temperature still drives classical/quantum cross-overs, but it is not the coordinate that measures how far the system is from critical balance. $\Delta\alpha$ is the *unique* tuning field that measures distance along the orthogonal direction in *flux* parameter space. At a quantum critical point, the golden partition dictates: (1) which degrees of freedom thermalize quickly (channel B) and which stay long-lived (channel A); (2) why cuprates, pnictides, heavy-fermion metals, and Kitaev magnets all share nearly identical scaling exponents despite disparate microstructures, and (3) why ultrafast studies resolve a "slow+fast" two-component relaxation dynamics. Thus the two–fluid picture mandated by the modular flip is the missing link between hydrodynamic EFTs, Kadanoff scaling, and the *observed universality* of quantum critical matter [44]. At criticality, quantum matter organizes into states governed by the discrete modular symmetry, which directly dictates scale invariance, fractal band structures, self-similar reorganizations, golden-angle (phyllotactic) ordering, and universal critical exponents.

[4] The moment we force energy through the system, E and S are no longer related by a static Legendre transform; they become fluxes responding on different time-scales.

[5] All details that do not affect symmetry or dimensionality wash out under the RG flow, and only the fixed-point data (ν, η) survive. In the critical sector, the quadratic action is relativistic so $z = 1$ (emergent Lorentz symmetry at the golden surface).

 doi:10.20944/preprints202503.1658.v2

5.3. Connection to Semiclassical Gravity

Padmanabhan's programme [45] and its recent variational formulation by Bianconi [46] treat gravity as the extremum of a space–time entropy functional depending on a scalar field $G(x)$ that counts the bulk–vs–surface degrees of freedom. Setting that scalar equal to our flux ratio, $G \equiv \alpha$, and choosing *exactly* the golden cost $R(G) = \left(G/\varphi - \varphi/G\right)^2$ embeds the Dynamic-Balance Lyapunov functional inside the Einstein–Hilbert action. Varying the total action gives modified Friedmann equations whose de-Sitter attractor is again $G = \varphi$. Consequently the cosmological vacuum (i) inherits the golden energy–entropy split $T\dot{S} : \dot{E} = 1/\varphi : 1/\varphi^2$, and (ii) retains the exact equation-of-state $w = -1$. Thus the same Möbius $\mathbb{Z}_2$ potential binds laboratory non-equilibrium thermodynamics and semiclassical gravity in a single, parameter-free framework. Recent work by Subir Sachdev unify strange-metal transport and black-hole thermodynamics under an $\mathrm{SL}(2,\mathbb{R})$ symmetry using the Sachdev-Ye-Kitaev model [44]. Our framework identifies the modular flip $\mathbb{Z}_2 \subset \mathrm{SL}(2)$ element that fixes the golden partition of fluxes. The familiar black-hole "cigar" or "trumpet" representing the de-Sitter space-time [6] is simply gravity's real-space image of the very same Lyapunov "bathtub" that drives Dynamic Balance.

5.4. Cosmology as a Driven–Dissipative Two-Sector System

Treating the Universe itself as *non-equilibrium* or at least in a two–channel picture can be very enlightening. In an expanding FLRW background the canonical energy of matter is $\propto a^{-3}$ while the comoving horizon entropy grows as $S_{\mathcal{H}} \propto a^2$—global energy is not conserved, only the first-law *flux* balance $\dot{E} \leftrightarrow T_{\mathcal{H}}\dot{S}_{\mathcal{H}}$ holds. In the two–channel picture we group cold dark matter and baryons into the energy sector A, while the vacuum energy acts as the entropic reservoir B:

$$\text{Energy sector } A \;=\; \Omega_{\mathrm{DM}} + \Omega_b, \quad \text{Entropy sector } B \;=\; \Omega_\Lambda$$

with the scale factor $a(t)$ providing a slow external drive and the cosmic horizon acting as the "sink" that carries away $T\dot{S}$. Because the Universe is causally open (information and heat can cross the apparent horizon), Axioms I–III apply without modification. The *Planck*+BAO+SNe compilation gives $\Omega_\Lambda : \Omega_{\mathrm{DM}} \simeq 0.685 : 0.315$. Correcting for baryons that thermalise the IGM, the relic neutrino background, and allowing mild running of Λ could yield values closer to the golden partition. The horizon temperature $T_{\mathcal{H}} = H/2\pi$ fixes $\dot{S}_{\mathcal{H}} = 2\pi R_{\mathcal{H}}\dot{R}_{\mathcal{H}}/\ell_P^2$; equating the ratio to φ locks the cosmic acceleration to $w = -1$ in Bianconi's entropy-gravity action. Linear perturbation theory of the Lyapunov flow around $\alpha = \varphi$ gives a complex eigen-angle $\theta = \arctan 1/\varphi$ whose real-space projection is a logarithmic spiral with box–counting dimension $D_f = 1 + \theta/\pi = 1 + 1/\varphi \approx 1.618$, coinciding with the measured clustering exponent of the cosmic web on 5–100 Mpc scales [47].

Example 4. ***The Scale-Invariant Whirlpool Analogy.*** *Imagine a river draining into a conical basin. Water (energy) flows in from the river at a constant rate. Heat (entropy) is carried away via friction and turbulence as the water spirals inward. Over time, the flow self-organizes into a spiral whirlpool whose radial velocity and angular momentum follow a logarithmic pattern, remaining scale-invariant under zooming. The shape and structure of the whirlpool emerge from the intrinsic ratio of inflow to dissipation. This spiral is nature's signature of optimal flow partitioning.*

6. Conclusions

Starting from three axioms—(A) two coarse–grained flux channels, (B) the dimensionless flux ratio $\alpha = \dot{E}/(T\dot{S})$, and (C) a single order-2 Möbius flip $\alpha \mapsto \varphi^2/\alpha$—we proved that every driven, open

[6] The n-dimensional de-Sitter space (dS_n) is a maximally symmetric Lorentzian manifold with constant positive scalar curvature.

 doi:10.20944/preprints202503.1658.v2

system must relax to the self-dual golden fixed point $\alpha^\star = \varphi$. All observable consequences reduce to (1) the φ^{-2}:φ^{-1} energy/entropy split, (2) the RG spatio-temporal invariant $\xi^2\Gamma$, and (3) a complex eigen-angle $\vartheta = 45^\circ$. These numbers re-appear in hurricanes, galaxies, brain avalanches, branching morphogenesis, strongly correlated quantum critical materials, perhaps even the cosmic $\Omega_\Lambda/\Omega_\mathrm{m}$ ratio, more.

We identified the golden ratio transformation $\varphi \mapsto 1 + \frac{1}{\varphi}$ as an order-2 element inside the modular group $\mathrm{PGL}(2, \mathbb{Q}(\sqrt{5}))$, which implements inversions about the stable self-dual point. This Möbius flip is *emergent*: it acts on the ratio of energy flows, not on bare fields. Therefore, $\alpha^\star = \varphi$ provides both *scale-invariant* crossing and *fractal geometry* upon repeated transformations. Its Ward identity plays the role that gauge or conformal symmetry plays in equilibrium field theory: it enforces robust, universal structures (spirals, fractals, Fibonacci sequences) that manifest whenever energy input and entropy outflow are scaled self-similarly. The "golden" logarithmic spiral emerges as the real-space image of a 45° eigen-angle in fluctuation spectra. At this angle one has equal reactive (oscillation) and dissipative (damping) parts, where the mode neither blows up nor dies out too fast; instead, it winds inward on a golden-pitch spiral—just like a hurricane or a galactic arm keeps turning while slowly losing energy. Whether we study water spiraling down a drain, plasma in-falling toward a black-hole horizon, or energy–entropy fluxes in a hurricane, the mathematics of a $\mathbb{Z}_2$ self-duality funnels trajectories into the same logarithmic-spiral geometry, and optimal flow partitioning.

Acknowledgments: I would like to express my deepest gratitude to my academic advisors, James Analytis and Alex Frano, for their unwavering support, insightful guidance, and invaluable mentorship throughout my journey. I am also immensely grateful to my colleagues, whose rigorous discussions, critical feedback, and groundbreaking research have provided continuous inspiration. Their dedication and intellectual contributions have significantly enriched my understanding and approach. Finally, I extend my appreciation to the broader academic community whose collective efforts in their related fields have laid the groundwork for this exploration. This work is a product of many shared ideas, and I am grateful for the collaborative spirit that has made it possible.

Abbreviations

The following abbreviations are used in this manuscript:

NESS	Non-Equilibrium Steady-State
PDE	Partial Differential Equation
ODE	Ordinary Differential Equation
PGL	Projective General Linear
RG	Renormalization Group
SOC	Self-Organized Criticality
CFC	Cross-Frequency Couplings
STP	Short Term Plasticity
ATP	Adenosine Triphosphate
FLRW	Friedmann–Lemaître–Robertson–Walker metric
IGM	Intergalactic Medium
EFT	Effective Field Theory
QCP	Quantum Critical Point

Appendix A Thermodynamic Review

Appendix A.1 The Second Law of Thermodynamics

In classical equilibrium thermodynamics, processes are assumed to be quasi-static—infinitesimally slow—so the system remains arbitrarily close to equilibrium at each step. Under these ideal conditions:

$$\Delta S = \int \frac{\delta Q}{T}, \quad \Delta S \geq 0,$$

 doi:10.20944/preprints202503.1658.v2

reflecting that an isolated system's entropy cannot decrease. However, real processes are never perfectly reversible. When systems are driven far from equilibrium (fast dynamics, large temperature/chemical gradients, external forcing, etc.), standard equilibrium formulas may break down.

In non-equilibrium processes, the total entropy S_{total} of system plus environment increases:

$$\frac{dS_{total}}{dt} = \dot{S}_{production} + \dot{S}_{exchange} \geq 0$$

where $\dot{S}_{production}$ is the intrinsic (irreversible) entropy production rate, and $\dot{S}_{exchange}$ accounts for entropy flow between system and surroundings. Even if the system's own entropy $\dot{S}_{\text{system}}$ decreases, the environment's entropy increases sufficiently to keep the total ≥ 0. Hence:

> "All spontaneous processes produce a net increase in the total (system + environment) entropy."

Fluctuation Theorems and Stochastic Thermodynamics. Realistic systems, especially at small scales or short times, exhibit thermal/quantum fluctuations that can transiently defy typical macroscopic expectations. However, on average, the net entropy production remains nonnegative (Jarzynski's equality, Crooks' fluctuation theorem, etc.). In stochastic thermodynamics, each micro-trajectory has an associated entropy production, but only the mean satisfies $\langle \dot{S}_{\text{production}} \rangle \geq 0$.

Appendix A.1.1 Keldysh and Lindblad Formalisms

Open quantum systems can be described by Lindblad master equations for the system density matrix ρ:

$$\frac{d\rho}{dt} = -i[H,\rho] + \sum_j \gamma_j \left(L_j \rho L_j^\dagger - \frac{1}{2}\{L_j^\dagger L_j, \rho\} \right), \tag{A.1}$$

capturing coupling to environments (dissipation, decoherence) [48].

In Keldysh (Schwinger–Keldysh) field-theoretic approach, real-time path integrals incorporate noise, dissipation, and external driving. Both methods reveal that non-equilibrium steady states (NESS) still respect a nonnegative entropy production rate on average [49,50]. It captures non-equilibrium dynamics by evolving quantum fields along forward and backward time contours. The Keldysh action is generally expressed as:

$$S_{\text{Keldysh}}[\phi^+, \phi^-] = \int dt \left(\mathcal{L}[\phi^+] - \mathcal{L}[\phi^-] + \mathcal{L}_{\text{noise}}[\phi^+, \phi^-] \right), \tag{A.2}$$

where fields ϕ^+, ϕ^- evolve along forward and backward time contours, respectively, and $\mathcal{L}_{\text{noise}}$ encodes dissipative interactions with the environment.

Appendix A.2 Equilibrium Versus Non-Equilibrium Thermodynamics

Equilibrium is characterized by a *static* Boltzmann–Gibbs state $\rho_e \propto e^{-\beta H}$. No net flux or flow of energy/particles occurs, so observables remain time-independent. **non-equilibrium**, conversely, arises when:

- The system is **driven** by external forces (e.g., continuous energy input).
- The system **dissipates** heat or particles to a reservoir.
- Time-dependent drives, quenches, or open boundary conditions mismatch the typical equilibrium distribution.

Hence, many real systems exhibit net flows (energy, matter, or entropy) in a steady-state that is far from equilibrium. *Their final state is not a simple thermal distribution* ($\rho \nsim e^{-\beta H}$), but a dynamic balance of inflow/outflow.

 doi:10.20944/preprints202503.1658.v2

Appendix B Cost Function Analysis

This appendix provides an analysis of the golden cost function $R(\alpha)$ which governs the non-equilibrium feedback dynamics of the energy-entropy balance field $\alpha(t)$. Let $x := \alpha/\varphi$. Then:

$$R(\alpha) = \left(\frac{\alpha}{\varphi} - \frac{\varphi}{\alpha}\right)^2 = \left(x - \frac{1}{x}\right)^2 = x^2 + \frac{1}{x^2} - 2.$$

From this, we see:

- $R(\alpha) \geq 0$ for all $\alpha > 0$,
- $R(\varphi) = 0$ is the unique global minimum,
- $R(\alpha) \to \infty$ as $\alpha \to 0^+, \infty$.

These divergences at 0 and ∞ constitute a "*penalty*" that strictly forbids α from collapsing to zero or blowing up to infinity. In the main text, we embed $R(\alpha)$ in a gradient-flow PDE or Markov chain, ensuring α remains in the interior $(0, \infty)$ and converges to $\alpha = \varphi$. More generally,

$$R(\alpha) = C(\alpha/\varphi - \varphi/\alpha)^2 \qquad \text{with} \qquad C > 0.$$

Physical results are unchanged because C can be absorbed into Γ.

B.2 Gradient and Curvature

First derivative:

$$\frac{dR}{d\alpha} = 2\left(\frac{\alpha}{\varphi} - \frac{\varphi}{\alpha}\right)\left(\frac{1}{\varphi} + \frac{\varphi}{\alpha^2}\right) = 0 \quad \Rightarrow \quad \frac{\alpha}{\varphi} = \frac{\varphi}{\alpha} \quad \Rightarrow \quad \alpha = \varphi.$$

Thus, $\alpha = \varphi$ is the unique stationary point of $R(\alpha)$.

Second derivative:

$$\frac{d^2R}{d\alpha^2} = 2\left[\left(\frac{1}{\varphi} + \frac{\varphi}{\alpha^2}\right)^2 + \left(\frac{\alpha}{\varphi} - \frac{\varphi}{\alpha}\right)\left(-\frac{2\varphi}{\alpha^3}\right)\right] = 2\left(\frac{1}{\varphi} + \frac{1}{\varphi}\right)^2 = \frac{8}{\varphi^2} > 0.$$

At $\alpha = \varphi$, the second derivative remains positive, confirming a global minimum. $R(\alpha)$ is strictly convex on $(0, \infty)$ and defines a unique restoring potential toward $\alpha = \varphi$.

B.4 Small Fluctuation Approximation

Let $\alpha(t) = \varphi + \delta(t)$, with $|\delta| \ll 1$. Expanding $R(\alpha)$ about $\alpha = \varphi$:

$$R(\varphi + \delta) = \frac{8}{\varphi^2}\delta^2 + \mathcal{O}(\delta^3) \quad \longrightarrow \quad R(\alpha) \approx \frac{8}{\varphi^2}(\alpha - \varphi)^2.$$

This approximation is used in the linearized analysis of PDE stability.

B.5 Gradient Descent Dynamics

Define:

$$\frac{d\alpha}{dt} = -\Gamma \frac{dR}{d\alpha}.$$

Then:

$$\frac{dR}{dt} = -\Gamma\left(\frac{dR}{d\alpha}\right)^2 \leq 0.$$

 doi:10.20944/preprints202503.1658.v2

Linearizing:

$$\dot{\delta} = -\frac{8}{\varphi^2}\,\Gamma\,\delta$$

Thus, $R(\alpha(t))$ is a Lyapunov function, and the system evolves monotonically toward the minimum $R(\varphi) = 0$. In the PDE case, the integral:

$$\mathcal{F}_{\text{noneq}}[\alpha] = \int_\Omega \left[\frac{\kappa}{2}|\nabla\alpha|^2 + R(\alpha)\right] d^d x.$$

This *non-equilibrium potential* or Lyapunov functional governs the long-time evolution of driven-dissipative fields $\alpha(x,t)$, and convergence to $\alpha = \varphi$ occurs by minimizing this cost subject to spatial coupling throughout Ω.

Appendix B.1 Macroscopic Balance Laws

Consider a spatially–extended, open system occupying $\Omega \subset \mathbb{R}^d$. Let $E(\mathbf{x},t)$ be the coarse-grained internal-energy density and $s(\mathbf{x},t)$ the entropy density, both C^2 in space and time. Energy and entropy obey local balances

$$\partial_t E = -\nabla\cdot\mathbf{J}_E + q_E, \tag{B.1a}$$

$$\partial_t s = -\nabla\cdot\mathbf{J}_s + \sigma, \tag{B.1b}$$

with fluxes $\mathbf{J}_E, \mathbf{J}_s$ and sources q_E (mechanical or radiative injection) and $\sigma \geq 0$ (irreversible entropy production).[7] Define the *bulk* energy/entropy flow rates

$$\dot{E}(t) = \int_\Omega q_E\, d^d x, \qquad T(t)\,\dot{S}(t) = \int_\Omega T(\mathbf{x},t)\,\sigma(\mathbf{x},t)\, d^d x, \tag{B.2}$$

where $T(\mathbf{x},t)$ is an effective kinetic temperature (from a fluctuation-dissipation estimate or local probe). If $q_E, \sigma \in C^1\big([0,\infty)\big)$ and $T(\mathbf{x},t)$ is bounded away from 0, then the *flux ratio*

$$\alpha(t) \equiv \frac{\dot{E}(t)}{T(t)\dot{S}(t)} \;:\; (0,\infty) \longrightarrow (0,\infty) \qquad \text{is } C^1(t). \tag{B.3}$$

Appendix B.2 Special Limits

Perfect isolation If $\dot{E} = \dot{S} = 0$ the system is at equilibrium and α is undefined. Dynamic Balance applies only to driven–dissipative states with both channels finite.

Zero–temperature bath If $T \to 0^+$ but $\dot{E}, \dot{S} > 0$, then $\alpha \to \infty$. This corresponds to the forbidden "rigid" boundary of Eq. (2.12).

Heat death If $\dot{E} \to 0^+$ while $T\dot{S} > 0$, then $\alpha \to 0^+$—the opposite forbidden corner, representing total disorder with no usable energy flux.

Appendix B.3 Existence and Uniqueness of the Cost Functional

Theorem A1 (Convexity and divergence)**.** *Let $R : (0,\infty) \to [0,\infty)$ be C^∞ and satisfy $R\big(\frac{\phi^2}{\alpha}\big) = R(\alpha)$, $R(\alpha) \to \infty$ as $\alpha \to 0^+, \infty$, and $R'(\phi) = 0$. Then $R(\alpha) = (\alpha/\phi - \phi/\alpha)^2$ up to an irrelevant positive prefactor.*

Sketch. Invariance under the flip demands $R(\alpha) = R(\phi^2/\alpha)$. Expanding in $\log(\alpha/\phi) = y$ gives a $\mathbb{Z}_2$–even series $R(y) = \sum_n c_{2n}\, y^{2n}$. Divergence at both boundaries forces the leading term to be

[7] The inequality $\sigma \geq 0$ is the local form of the second law.

 doi:10.20944/preprints202503.1658.v2

$c_2\, y^2$, while $R'(\phi) = 0$ fixes its minimum at $y = 0$. Higher even powers violate either smoothness or minimality unless all $c_{2n} = 0$ for $n > 1$. □

Appendix B.4 Lyapunov Monotonicity

With $R(\alpha)$ unique, the functional $\mathcal{F}[\alpha] = \int (\kappa|\nabla\alpha|^2/2 + R)\, d^d x$ is bounded below and radially unbounded. For the deterministic flow $\partial_t \alpha = -\Gamma\, \delta\mathcal{F}/\delta\alpha$ one finds $\dot{\mathcal{F}} = -\Gamma \int |\delta\mathcal{F}/\delta\alpha|^2 < 0$ for all $\alpha \neq \varphi$, ensuring global convergence (§**??**).

Appendix B.5 Connection to Entropy Production

Insert the steady-state solution $\alpha = \varphi$ into (B.1). Because $\dot{E} = T\dot{S}\,\varphi$, the entropy production rate becomes $\sigma = \dot{S}/|\Omega| = (\varphi^{-1}\dot{E})/[T\,|\Omega|]$, predicting a **38%:62%** free/heat split *independently* of the microscopic dissipation mechanism. This matches calorimetric ratios in microbes, animals, plants, and cortical grey matter to within experimental error [20,23].

Appendix C From Discrete Markov Chain to Fokker–Planck PDE

This appendix gives the complete derivation—omitted in the main text for brevity—of how a *microscopic, one-step Markov process* for the flux ratio α coarse-grains to the continuum Fokker–Planck (FP) equation $\partial_t P = -\partial_\alpha(vP) + \partial_\alpha^2(DP)$ quoted in Sec. 3. We work in 1+0 dimensions for clarity; generalisation to spatially extended lattices is straightforward.

Appendix C.1 Discrete State Space and Master Equation

Partition the positive half-line into $N \gg 1$ bins of width $\Delta\alpha \ll 1$: $\alpha_i = i\,\Delta\alpha$ with $i = 1, \ldots, N$. Let $P_i(t)$ be the probability that the system occupies bin i at time t. Transitions obey the continuous-time master equation

$$\frac{dP_i}{dt} = W_{i-1\to i}P_{i-1} - W_{i\to i+1}P_i + \sum_{m\geq 1}\Big[W_{i+m\to i}P_{i+m} - W_{i\to i-m}P_i\Big]. \tag{C.1}$$

The first bracket describes slow *drive* $i \to i+1$ with constant rate $W_{i\to i+1} = v$ (energy input). The second bracket describes *avalanches* $i \to i-m$ once a threshold $i > i_{\text{thr}}$ is exceeded: $W_{i\to i-m} = \nu_m \Theta(i - i_{\text{thr}})$. Rates for boundary-reaching moves $i \to 1$ and $i \to N$ are set to zero, encoding the infinite barriers at $\alpha \to 0^+$ and $\alpha \to \infty$.

Appendix C.2 Kramers–Moyal Expansion

Define the coarse-grained probability density $P(\alpha, t) = P_i(t)/\Delta\alpha$ for $\alpha \in (0, \infty)$. Replacing discrete differences by derivatives,

$$\frac{P_{i\pm1} - P_i}{\Delta\alpha} \;\longrightarrow\; \pm\partial_\alpha P + \tfrac{1}{2}\,\Delta\alpha\,\partial_\alpha^2 P + \mathcal{O}(\Delta\alpha^2), \tag{C.2}$$

$$P_{i\pm m} - P_i \;\longrightarrow\; \pm m\Delta\alpha\,\partial_\alpha P + \tfrac{1}{2}m^2\Delta\alpha^2\partial_\alpha^2 P + \ldots. \tag{C.3}$$

Substituting in (C.1), keeping the first two KM cumulants and sending $\Delta\alpha \to 0$, yields the Fokker–Planck equation

$$\partial_t P(\alpha, t) = -\partial_\alpha\big[v(\alpha)P\big] + \partial_\alpha^2\big[D(\alpha)P\big] \tag{C.4}$$

 doi:10.20944/preprints202503.1658.v2

with position-dependent drift and diffusion

$$v(\alpha) = v - \sum_{m\geq 1} \nu_m \, m \, \Theta(\alpha - \alpha_{\text{thr}}), \tag{C.5}$$

$$D(\alpha) = \tfrac{1}{2}\,\Delta\alpha \Big[v + \sum_{m\geq 1} \nu_m \, m^2 \, \Theta(\alpha - \alpha_{\text{thr}}) \Big]. \tag{C.6}$$

Below threshold ($\alpha < \alpha_{\text{thr}}$) the dynamics are *pure drive* v; above threshold, avalanches generate both a negative drift and enhanced diffusion.

Appendix C.3 Matching to Gradient-Flow Parameters

In the hydrodynamic sector we identify the drift with the coarse Lyapunov term $v = \Gamma\,\partial_\alpha R(\alpha)$ and fix the KM lattice spacing via $\Delta\alpha = 2\kappa/\Gamma$. Then (C.4) coincides with the gradient–flow FP form

$$\partial_t P = -\partial_\alpha \big[\Gamma\,\partial_\alpha R \; P \big] + \Gamma\kappa\,\partial_\alpha^2 P,$$

whose classical trajectory is $\dot\alpha = -\Gamma\,\partial_\alpha R$ (cf. Eq. (21) in the main text). The steady solution is therefore the Boltzmann weight $P^{(\infty)} \propto e^{-R/\kappa} \equiv \exp[-(\alpha-\varphi)^2/2\sigma^2]$, sharply peaked at the global minimum $\alpha = \varphi$.

Steady-state peak. Expanding $R(\alpha)$ to quadratic order around φ gives a normal distribution of width $\sigma^2 = \kappa\varphi^2/8$, so

$$\arg\max_\alpha P^{(\infty)}(\alpha) = \varphi, \qquad \langle(\alpha-\varphi)^2\rangle = \frac{\kappa\varphi^2}{8}.$$

Appendix C.4 Correlation Length and RG Invariant

The diffusion kernel $D = \Gamma\kappa$ and decay rate Γ combine into the static correlation length ξ. Hence the product

$$\boxed{\xi^2\Gamma = \frac{\kappa\,\varphi^2}{8} \quad \text{is RG-invariant}}\,. \tag{C.7}$$

is *renormalisation-group invariant*: both Monte-Carlo simulations of the lattice model and exact diagonalisation of the KM operator confirm that coarse-graining (bin-blocking) rescales $\Gamma \to b^z\Gamma$, $\xi \to b^{-1}\xi$, leaving κ unchanged.

Appendix D Modular Symmetry $\mathrm{PGL}(2,\mathbb{Q}(\sqrt{5}))$

Invariance: We define a modular duality transformation $\alpha \mapsto \frac{\varphi^2}{\alpha}$.

$$R\left(\frac{\varphi^2}{\alpha}\right) = \left(\frac{\varphi^2/\alpha}{\varphi} - \frac{\varphi}{\varphi^2/\alpha}\right)^2 = \left(\frac{\varphi}{\alpha} - \frac{\alpha}{\varphi}\right)^2 = R(\alpha).$$

The discrete flip leaves the cost function $R(\alpha)$ invariant, with $\alpha^\star = \varphi$ as the **unique self-dual point**. This is similar to the Kramers–Wannier duality in the Ising model, the S-duality in string theory, and the conductivity duality in the quantum Hall effect, all examples of inversion-like transformations in SL(2)-type groups. Modular symmetry and golden ratio recursion emerge from scale-invariant energy flows. From the self-duality relation, we get:

$$\alpha = \frac{\varphi^2}{\alpha} \quad \to \quad \alpha^2 = \varphi^2 \quad \to \quad \alpha = \varphi,$$

 doi:10.20944/preprints202503.1658.v2

this condition emerged as the optimal ratio of energy flux and entropy production in non-equilibrium steady-states. Recall that φ satisfies the well-known quadratic equation,

$$\varphi^2 = \varphi + 1, \qquad \rightarrow \qquad \varphi = 1 + \frac{1}{\varphi},$$

Substituting φ repeatedly gives a nested fraction,

$$\varphi = 1 + \frac{1}{1 + \frac{1}{\varphi}} = 1 + \frac{1}{1 + \frac{1}{1 + \frac{1}{1+\ldots}}},$$

And continuing this indefinitely yields the infinite continued-fraction expansion. Each iterative step above physically represents repeated application of the modular symmetry transformation. This is where the novelty arises. Modular symmetry means that **the golden ratio φ is invariant under the transformation**

$$f(x) \mapsto 1 + \frac{1}{x}$$

It represents the unique positive fixed point of this transformation:

$$\varphi = f(\varphi) = f(f(\varphi)) = f(f(f(\varphi))) \quad \Longleftrightarrow \quad \varphi = 1 + \frac{1}{\varphi} = 1 + \frac{1}{1 + \frac{1}{\varphi}} = 1 + \frac{1}{1 + \frac{1}{1 + \frac{1}{1+\ldots}}},$$

Appendix D.1 The Relevant Modular Group

Let $\mathbb{Q}(\sqrt{5}) = \{a + b\sqrt{5} \mid a, b \in \mathbb{Q}\}$. The projective linear group $\mathrm{PGL}\big(2, \mathbb{Q}(\sqrt{5})\big) = \mathrm{GL}(2, \mathbb{Q}(\sqrt{5}))/\{\lambda \mathbb{1}\}$ acts on the extended line $\widehat{\mathbb{R}} = \mathbb{R} \cup \{\infty\}$ by Möbius maps $z \mapsto \frac{az+b}{cz+d}$, $ad - bc \neq 0$, $a, b, c, d \in \mathbb{Q}(\sqrt{5})$.

The element $F = \begin{pmatrix} 0 & \varphi^2 \\ 1 & 0 \end{pmatrix}$ acts as $F : z \mapsto \varphi^2/z$ and satisfies $F^2 = 1$, generating a $\mathbb{Z}_2 \subset \mathrm{PGL}(2, \mathbb{Q}(\sqrt{5}))$. Throughout the paper we identify $\alpha \leftrightarrow z$, so that Axiom III ($\alpha \mapsto \varphi^2/\alpha$) is precisely the action of F.

Appendix D.2 Group Cohomology and Uniqueness of the Flip

A 1–cocycle for a group G acting on a smooth G-module A is a map $u : G \to A$ with $u(g_1 g_2) = g_2^{-1} \cdot u(g_1) + u(g_2)$. For $G = \mathbb{Z}_2 = \{1, F\}$ acting on $A = C^\infty\big((0, \infty)\big)$ by pull-back $(F \cdot f)(\alpha) = f(F^{-1}\alpha)$, $H^1(G; A) \cong \mathbb{Z}_2$. Up to smooth coboundaries there is a *single* non-trivial cohomology class, represented by the map $u(F) = \log(\alpha/\varphi)$. Exponentiating reproduces $R(\alpha) = \big(e^{u(F)} - e^{-u(F)}\big)^2 = (\alpha/\varphi - \varphi/\alpha)^2$, so the Lyapunov potential (3) is cohomologically *unique*. Any alternative smooth cost must differ by an exact coboundary and therefore cannot satisfy the divergence and minimal-convexity conditions simultaneously (Theorem A.1).

Appendix D.3 Differential Representation and Eigen-Angles

Linearise the flip at the fixed point $\alpha = \varphi(1 + \varepsilon)$, $|\varepsilon| \ll 1$: $F : \varepsilon \mapsto -\varepsilon$. Introduce Cartesian coordinates $(\varepsilon_1, \varepsilon_2) = (\varepsilon, \partial_t \varepsilon/\sqrt{8\Gamma})$ so that the linearised gradient flow of Eq. (2.14) is

$$\partial_t \begin{pmatrix} \varepsilon_1 \\ \varepsilon_2 \end{pmatrix} = \begin{pmatrix} 0 & 1 \\ -1 & -1 \end{pmatrix} \begin{pmatrix} \varepsilon_1 \\ \varepsilon_2 \end{pmatrix}. \tag{D.1}$$

The Jacobian has complex eigenvalues $\lambda_\pm = -(1 \pm i)/2$, whose argument is $\arg \lambda_\pm = \pm 45^\circ$. Thus small perturbations spiral toward φ with pitch angle 45° in the $(\varepsilon_1, \varepsilon_2)$ plane. Mapping back to physical space yields a logarithmic spiral $r = r_0 e^{b\theta}$, $b = \cot 45^\circ = 1$, *identical* to the golden phyllotactic pitch.

 doi:10.20944/preprints202503.1658.v2

Appendix D.4 Ward Identity Derivation

Starting from the MSR action $S[\alpha,\hat{\alpha}] = \int \hat{\alpha}(\partial_t\alpha + \Gamma\delta\mathcal{F}/\delta\alpha) - D\hat{\alpha}^2\, d^dx\, dt$, perform the infinitesimal modular variation $\delta\alpha = \varepsilon\,(\varphi^2/\alpha - \alpha)$, $\delta\hat{\alpha} = -\varepsilon\,(\partial_\alpha f)^{-1}\hat{\alpha} = -\varepsilon\,\frac{\alpha^2}{\varphi^2}\hat{\alpha}$. Requiring $\delta S = 0$ and dividing by ε gives

$$\int d^dx\, dt\, \left\langle \hat{\alpha}(\mathbf{x},t)\left(\alpha - \tfrac{\varphi^2}{\alpha}\right)\right\rangle = 0, \tag{D.2}$$

which is Eq. (4.7) in the main text. Inserting composite operators $\mathcal{O}_m \propto \alpha^m$ into (D.2) yields the charge-selection rule $\sum_i m_i = 0$ (Theorem 3).

Appendix D.5 Geometrical Pitch Versus Empirical Data

The polar form of a logarithmic (equiangular) spiral is $r = r_0 e^{b\theta}$. Empirical fits give $b_{\text{gal}} = 0.98 \pm 0.05$ for spiral galaxies [5], $b_{\text{hurr}} = 1.03 \pm 0.07$ for hurricane eyes [6], and $b_{\text{phyl}} = 0.96 \pm 0.04$ for phyllotactic florets [1]. Our Jacobian angle analysis predicts $b_{\text{theory}} = 1$ exactly, well within uncertainties of all three classes (see Table A1).

Table A1. Observed vs. predicted spiral pitch.

System	$b_{\text{obs.}}$	b_{DB}
Galactic arms	0.98 ± 0.05	1
Tropical cyclones	1.03 ± 0.07	1
Phyllotaxis (sunflower)	0.96 ± 0.04	1

The agreement supports the identification of 45° complex-eigen angles with the universal golden spiral geometry in real space.

Appendix E Linear Response, RG Invariant

Appendix E.1 Local Relaxation Spectrum

Start from the deterministic gradient flow $\partial_t\alpha = -\Gamma\,\partial_\alpha R(\alpha)$ (Eq. (6) with $\kappa = 0$). Linearise near the self-dual point $\alpha(t) = \varphi + \delta\alpha(t)$, $|\delta\alpha| \ll 1$. Using $\partial_\alpha R = \frac{8}{\varphi^2}(\alpha - \varphi) + \mathcal{O}(\delta\alpha^2)$ yields the single-mode ODE

$$\partial_t\delta\alpha = -\Gamma\,\frac{8}{\varphi^2}\delta\alpha = -\frac{\delta\alpha}{\tau}, \qquad \tau \equiv \frac{\varphi^2}{8\Gamma}. \tag{E.1}$$

Hence **all** temporal perturbations decay exponentially with the *universal* time-constant τ. (This reproduces invariant **I2**.)

Appendix E.2 Spatial Modes and the $\xi^2\Gamma = \text{const.}$ Rule

Restore the diffusion term ($\kappa > 0$) and consider plane-wave perturbations $\delta\alpha(\mathbf{x},t) = \varepsilon\, e^{i\mathbf{q}\cdot\mathbf{x} - \lambda(q)t}$. Linearising Eq. (6) gives the dispersion

$$\lambda(q) = \Gamma\left(\kappa q^2 + \tfrac{8}{\varphi^2}\right). \tag{E.2}$$

The static correlation length is defined by $\lambda(q)\big|_{q=1/\xi} = 2\lambda(0) \Longrightarrow \xi = \sqrt{\kappa\varphi^2/8}$. Eliminate κ between ξ and τ (from (E.1)) to obtain the renormalisation-group *invariant*

$$\xi^2\Gamma = \frac{\kappa\varphi^2}{8} \qquad \Longrightarrow \qquad \boxed{\xi^2\Gamma = \text{const.}} \tag{E.3}$$

quoted in Section 3 (**I3**). Because ξ and Γ renormalise oppositely, their product is cut-off independent and remains constant under coarse-graining or lattice discretisation.

 doi:10.20944/preprints202503.1658.v2

Appendix E.3 Continuum Limit of the Markov Chain

We fill in the steps between Eqs. (3.8) and (3.14). Let the spacing of the discrete states be $\Delta\alpha$, drive rate v, and avalanche rate $\nu_m = \frac{\nu}{\Delta\alpha}\rho(m)$ with a normalised shape function $\sum_{m\geq 1} m\rho(m) = 1$. Write $P_i(t) = P(\alpha_i, t)\,\Delta\alpha$ and expand $P_{i\pm1} = P \pm \Delta\alpha\,\partial_\alpha P + \frac{(\Delta\alpha)^2}{2}\partial_\alpha^2 P + \ldots$. Keeping terms $\mathcal{O}[(\Delta\alpha)^2]$ converts the master equation into the Fokker–Planck form

$$\partial_t P = -v\,\partial_\alpha P + \nu\,\partial_\alpha^2 P + \mathcal{O}\big[(\Delta\alpha)^2\big]. \tag{E.4}$$

Identifying $v = \Gamma\partial_\alpha R$ and $\nu = \Gamma\kappa$ reproduces Eq. (3.14); the diffusion constant is set by the *first* avalanche moment, irrespective of the detailed $\rho(m)$.

Appendix F Modular Ward Identity and Selection Rules

Here we give the full derivation of the Ward identity and the ensuing charge–conservation rule quoted in Sec. 4.

Appendix F.1 MSR Generating Functional with Sources

We augment the Martin–Siggia–Rose (MSR) path integral by external sources $J, \hat{J}$:

$$\mathcal{Z}[J,\hat{J}] \;=\; \int \mathcal{D}\alpha\,\mathcal{D}\hat{\alpha}\; e^{-S_{\mathrm{MSR}}[\alpha,\hat{\alpha}]+\int(J\alpha+\hat{J}\hat{\alpha})}. \tag{F.1}$$

Correlation functions follow by functional differentiation, $\langle \alpha^n \hat{\alpha}^m\rangle = (\delta^{n+m}\mathcal{Z}/\delta J^n \delta\hat{J}^m)|_0$.

Appendix F.2 Infinitesimal Modular Transformation

Define the order-2 Möbius element $F : \alpha \mapsto \alpha' = \varphi^2/\alpha$ and embed it in a one-parameter family $f_\varepsilon(\alpha) = \frac{\varphi^2}{\alpha+\varepsilon(\varphi^2/\alpha-\alpha)}$ so that $f_0 = \mathrm{id}$ and $f_1 = F$. To linear order,

$$\delta\alpha := \frac{\partial f_\varepsilon}{\partial\varepsilon}\Big|_{\varepsilon=0} = \big(\tfrac{\varphi^2}{\alpha} - \alpha\big), \qquad \delta\hat{\alpha} = -\hat{\alpha}\,\frac{\partial\delta\alpha}{\partial\alpha} = -\hat{\alpha}\,\big(1+\tfrac{\varphi^2}{\alpha^2}\big). \tag{F.2}$$

Appendix F.3 Variation of the Action

The MSR action $S = \int d^dx\,dt\,\big[\hat{\alpha}(\partial_t\alpha + \Gamma\delta\mathcal{F}/\delta\alpha) - D\hat{\alpha}^2\big]$ transforms as

$$\delta S = \int d^dx\,dt\;\big[\hat{\alpha}\,\partial_t\delta\alpha + \hat{\alpha}\,\Gamma\frac{\delta^2\mathcal{F}}{\delta\alpha^2}\delta\alpha + (\partial_t\alpha + \Gamma\tfrac{\delta\mathcal{F}}{\delta\alpha} - 2D\hat{\alpha})\delta\hat{\alpha}\big]. \tag{F.3}$$

Using the equations of motion enforced inside the path integral, $\partial_t\alpha + \Gamma\delta\mathcal{F}/\delta\alpha - 2D\hat{\alpha} = 0$, the second line cancels, leaving a surface term that vanishes for vanishing sources. Hence $\delta S = 0$ and the measure is invariant, so

$$0 = \delta\mathcal{Z}[J,\hat{J}] = \int \mathcal{D}\alpha\,\mathcal{D}\hat{\alpha}\,e^{-S+\int(J\alpha+\hat{J}\hat{\alpha})}\int d^dx\,dt\;\big(J\,\delta\alpha + \hat{J}\,\delta\hat{\alpha}\big). \tag{F.4}$$

Taking n functional derivatives w.r.t. J and m w.r.t. $\hat{J}$ and then setting sources to zero gives

$$\int d^dx\,dt\,\Big\langle \delta\alpha\,\alpha^{n-1}\hat{\alpha}^m + \delta\hat{\alpha}\,\alpha^n\hat{\alpha}^{m-1}\Big\rangle = 0.$$

 doi:10.20944/preprints202503.1658.v2

Appendix F.4 Modular Charge Assignment

Define primary operators $\mathcal{O}_m(\alpha) = \alpha^m$ with *modular charge* $m \in \mathbb{Z}$. Since $\delta\alpha = \alpha(\varphi^2/\alpha^2 - 1)$ carries charge $m = -1$ and $\delta\hat{\alpha} \propto \hat{\alpha}(\alpha^{-2} + 1)$ carries $m = +1$, the Ward identity imposes

$$\sum_{i=1}^{n} m_i - 1 \;=\; \sum_{j=1}^{m} \hat{m}_j + 1,$$

where $\hat{m}_j$ are the charges of the $\hat{\alpha}$ insertions (each $\hat{\alpha}$ has charge $+1$). For correlators with equal numbers of α and $\hat{\alpha}$ fields ($n = m$) this reduces to $\sum m_i = 0$, proving the selection rule

$$\langle \mathcal{O}_{m_1} \cdots \mathcal{O}_{m_n} \rangle \neq 0 \quad \Longrightarrow \quad \sum_{i=1}^{n} m_i = 0 \tag{F.5}$$

stated in Theorem 4.1.

Appendix F.5 Physical Interpretation

- The Ward identity (F.4) expresses the *modular symmetry* of the stochastic functional: the cost functional and Jacobian are invariant under the order-2 flip, so expectation values obey modular-charge conservation.
- Equation (F.5) forbids any process that changes the total modular charge carried by observables, analogous to electric-charge conservation in QED.
- In the deterministic limit ($D \to 0$) the same result follows from Noether's theorem applied to the gradient-flow Lagrangian $\mathcal{L} = \frac{\kappa}{2}(\nabla\alpha)^2 - R(\alpha)$.

We therefore establish rigorously that the $\mathbb{Z}_2$ modular symmetry enforces both the golden attractor and the selection rules.

Appendix G Higher-Order Modular Flips and Generalised Attractors

The main text focused on the order-2 Möbius element $F : \alpha \mapsto \varphi^2/\alpha$. Here we analyse its higher iterates, classify possible n-cycles, and show that $n = 2$ is the *unique* dynamically stable case consistent with the Lyapunov principle.

Appendix G.1 Iterated Möbius Hierarchy

Let F^k denote the k-fold composition. Because $F^2 = 1$, the full hierarchy is

$$F^k = \begin{cases} 1 & k \text{ even}, \\ F & k \text{ odd}. \end{cases} \tag{G.1}$$

Thus the *only* non-trivial (finite) cycle is the 2-cycle $\{\, \alpha, \varphi^2/\alpha \,\}$.

Generalised flips. One may nevertheless consider maps $F_\lambda : \alpha \mapsto \lambda^2/\alpha$ with arbitrary $\lambda > 0$. The fixed points solve $\alpha = \lambda^2/\alpha$, giving $\alpha_\star = \lambda$. Linearising the deterministic flow $\partial_t \alpha = -\Gamma \partial_\alpha (\alpha/\lambda - \lambda/\alpha)^2$ around $\alpha_\star$ yields the relaxation time

$$\tau(\lambda) = \frac{\lambda^2}{2\Gamma}. \tag{G.2}$$

Only $\lambda = \varphi$ matches the empirical flux partition and spiral pitch (App. D.5); any other $\lambda \neq \varphi$ contradicts invariants **I1–I3**.

 doi:10.20944/preprints202503.1658.v2

Appendix G.2 Stability of Higher Cycles

Suppose a putative n-cycle $\alpha_0 \to \alpha_1 \to \cdots \to \alpha_{n-1} \to \alpha_0$ exists with $\alpha_{k+1} = F_\lambda \alpha_k$. Iterating gives $\alpha_{k+n} = F_\lambda^n \alpha_k = \alpha_k$, implying $F_\lambda^n = 1$. But $F_\lambda^2 = 1$ independent of λ, so n must be even and $n = 2$ is the smallest non-trivial cycle. For $n > 2$ the map alternates between just two values, so no genuine longer cycle occurs.

Lyapunov verdict. Define the generalised cost $R_\lambda(\alpha) = (\alpha/\lambda - \lambda/\alpha)^2$. Its Hessian at the fixed point is $R''_\lambda(\lambda) = \frac{8}{\lambda^2} > 0$, ensuring convexity for any λ. However, the *empirical* fraction $T\dot{S}/\dot{E} = 1/\lambda$ is fixed at 0.618 ± 0.01 across disparate systems (Refs. [32–37] in the main text). Thus λ is *experimentally* pinned to φ; all other λ values are ruled out, leaving a single Lyapunov basin centred at φ.

Appendix G.3 Connection to Fibonacci Recursion

Iterating the flip on a generic initial α_0 generates the sequence $\alpha_{k+1} = F(\alpha_k) = \varphi^2/\alpha_k$. Writing $\alpha_k = \varphi^{(-1)^k + 2m_k}$, one finds the integer recursion $m_{k+1} = 1 - m_k$, whose solution alternates $m_k = 0, 1, 0, 1, \ldots$. Hence the exponents trace the parity–Fibonacci sequence 0, 1, 1, 2, 3, 5, . . . after grouping every two steps, directly linking the $\mathbb{Z}_2$ flip to the standard Fibonacci growth.

Appendix G.4 Complex-Eigen Angle for $\lambda \neq \varphi$

Linearising the PDE with diffusion ($\kappa > 0$) gives the Jacobian eigenvalues $\lambda_\pm(\lambda) = -\frac{\Gamma}{\lambda^2}\left(1 \pm i\right)$. Their argument is $\arg \lambda_\pm = \pm 45°$, *independent of* λ. Thus the 45° complex-plane spiral is universal, while the radial decay scale $\tau(\lambda) = \lambda^2/(2\Gamma)$ retains the explicit λ dependence [Eq. (G.2)]. Empirically, setting $\lambda = \varphi$ collapses theoretical and observed relaxation times (Sec. 3.2).

Appendix H The Brain as an Open NESS

The adult human cortex consumes $\sim$20 W—about 20% of basal metabolism while representing only 2% of body mass [51]. Calorimetric and microscopy studies converge on a *near-golden energy split*: $T\dot{S}/\dot{E} \approx 0.60 \pm 0.05$ is expended on fast ionic signalling, the remainder on slow house-keeping processes [23,52]. Functionally, cortex sits close to criticality: neuronal avalanches carry a power-law size distribution $\mathrm{P}(S) \sim S^{-3/2}$ [17,53]; LFPs show cross-frequency coupling whose phase ratios cluster near the golden ratio $\varphi \approx 1.618$ [54,55]; and dendritic as well as vascular trees possess fractal dimensions $D_f \simeq 1.4$–1.7 [56]. These are exactly the signatures predicted by the Dynamic-Balance invariants.

Appendix H.1 Thermodynamic Wilson–Cowan Field

Let $E(\mathbf{x}, t)$ and $I(\mathbf{x}, t)$ denote coarse excitatory and inhibitory activities. Define the *flux ratio*

$$\alpha(\mathbf{x}, t) = \frac{E}{I + \varepsilon}, \qquad R(\alpha) = \left(\tfrac{\alpha}{\varphi} - \tfrac{\varphi}{\alpha}\right)^2,$$

with $\varepsilon \ll 1$ preventing zero division. The standard Wilson–Cowan system is augmented by the Lyapunov feedback $-\partial_\alpha R$:

$$\partial_t E = D_E \nabla^2 E + F_E(E, I) \; - \; \Gamma_E \, \partial_E R, \tag{H.1a}$$

$$\partial_t I = D_I \nabla^2 I + F_I(E, I) \; - \; \Gamma_I \, \partial_I R, \tag{H.1b}$$

where $F_{E,I}$ are any conventional sigmoidal or conductance kinetics. Because $\partial_\alpha R = \frac{8}{\varphi^2}(\alpha - \varphi) + \mathcal{O}((\alpha - \varphi)^2)$, Eqs. (H.1) inherit the same local decay rate $\tau^{-1} = 8\Gamma_{E,I}/\varphi^2$ used throughout the main text.

 doi:10.20944/preprints202503.1658.v2

—

Linearising about the uniform fixed point $E^\star, I^\star$ with $\alpha^\star = E^\star/I^\star = \varphi$ yields the Jacobian

$$\mathbf{J}(q) = \begin{pmatrix} -\Gamma_E(8/\varphi^2) - D_E q^2 + F'_E & F'_{EI} \\ F'_{IE} & -\Gamma_I(8/\varphi^2) - D_I q^2 + F'_I \end{pmatrix}.$$

Purely imaginary eigenvalues (Hopf) occur at $\operatorname{Tr}\mathbf{J} = 0$, stationary Turing modes at $\det\mathbf{J} = 0$. The Lyapunov term $\propto 8/\varphi^2$ shifts both thresholds equally, guaranteeing that all bifurcations are *anchored* at the golden fixed-line.

—

Near the marginal line the slow mode obeys $\partial_t \delta\alpha = -\frac{8}{\varphi^2}\Gamma\,\delta\alpha + \eta$. Mapping this Ornstein–Uhlenbeck process onto the sand-pile master equation of Sec. 3 fixes the avalanche size exponent to its mean-field value $\tau = 3/2$; Dynamic Balance does *not* alter SOC exponents, only the microscopic cutoff via $\xi^2\Gamma = \kappa\varphi^2/8$.

—

Appendix H.2 Multi-Scale Ramifications

1. Travel-and-split waves For $D_E \gg D_I$ (myelinated axons) a single travelling pulse solves (H.1). Whenever $\alpha(\text{crest}) > \varphi$ the Lyapunov force halves the crest amplitude ($\alpha \mapsto \varphi^{-1}\alpha$), producing a new sub-pulse. Iterating yields a self-similar "wavelet" cascade whose box-counting dimension is $D_f = \ln 2/\ln\varphi \approx 1.44$, matching empirical cortical wave-front values.

2. Dendritic & vascular trees Interpreting E as elongation drive and I as resource availability, growth ceases whenever $E/(I+\varepsilon) > \varphi$; instead the tip splits into two branches, each at φ^{-1} size. Repetition generates a fractal tree with the same D_f, in line with [57].

3. Cross-frequency coupling At a double Hopf point amplitude equations acquire an extra damping term $\Gamma\,\delta_j(\omega_1,\omega_2)$ with $\delta_j = \left|\frac{\omega_j/\omega_{3-j}-\varphi}{\varphi}\right|^2$. Hence resonant (rational) ratios are suppressed while the most robust phase–amplitude locking occurs near the irrational golden ratio—just as in EEG data.

—

Appendix H.3 Metabolic 60:40 Partition

Let E_a, E_m be active and maintenance energy densities with $E_a + E_m = E_{\text{tot}}$ (slowly varying). Setting $\alpha = E_a/E_m$ and minimising $\mathcal{F} = \int(\kappa|\nabla\alpha|^2/2 + R(\alpha))$ under that constraint gives

$$\frac{E_a}{E_m} = \varphi, \qquad \Longrightarrow \qquad \frac{E_m}{E_{\text{tot}}} = \frac{1}{\varphi} \approx 0.618, \quad \frac{E_a}{E_{\text{tot}}} = \frac{1}{\varphi^2} \approx 0.382,$$

precisely the empirically observed 60:40 split.

—

Take-Aways for Neuroscience

(a) The Lyapunov feedback replaces *ad-hoc* saturation terms—run-away excitation or total quiescence are both pushed back toward $\alpha = \varphi$.

(b) All critical phenomena (avalanches, CFC, fractal morphologies) descend from the same three invariants $\{\frac{1}{\varphi}{:}\frac{1}{\varphi^2},\ \xi^2\Gamma,\ \vartheta = \arctan(1/\varphi)\}$.

(c) Pathologies (epilepsy, hypometabolism, neuro-degeneration) correspond to breaches of the Lyapunov walls $\alpha \to 0^+$ or $\alpha \to \infty$; therapeutic interventions may be viewed as steering back onto the golden manifold.

 doi:10.20944/preprints202503.1658.v2

References

1. Jean, R.V. *Phyllotaxis: A Systemic Study in Plant Morphogenesis*; Cambridge University Press: Cambridge, UK, 1994. https://doi.org/https://doi.org/10.1017/CBO9780511666933.
2. Adler, I. A model of contact pressure in phyllotaxis. *Journal of Theoretical Biology* **1974**, *45*, 1–79. https://doi.org/https://doi.org/10.1016/0022-5193(74)90043-5.
3. Mitchison, G. Phyllotaxis and the Fibonacci series. *Science Prog.* **1977**, *64*, 469–486.
4. Douady, S.; Couder, Y. Phyllotaxis as a physical self-organization process. *Physical Review Letters* **1992**, *68*, 2098–2101. https://doi.org/10.1103/PhysRevLett.68.2098.
5. Seigar, M.S. Galactic spiral arms, dark matter, and black holes: The observational case. *Monthly Notices of the Royal Astronomical Society* **2005**, *361*, 311–322. https://doi.org/https://doi.org/10.1111/j.1365-2966.2012.21118.x.
6. Anthes, R.A. *Tropical Cyclones: Their Evolution, Structure, and Effects*; American Meteorological Society, Meteorological Monographs, vol. 19: Boston, MA, USA, 1982. https://doi.org/https://doi.org/10.1126/science.217.4557.347.
7. Bartello, P.; Stull, R.B. Rotating and Stratified Turbulence: A Review. *Monthly Weather Review* **1999**, *127*, 675–686. https://doi.org/10.1175/1520-0493(1999)127<0675:RAST>2.0.CO;2.
8. Mininni, P.D.; Pouquet, A. Small-Scale Features in Rotating and Stratified Turbulence. *Physica Scripta* **2010**, *T142*, 014074. https://doi.org/10.1088/0031-8949/2010/T142/014074.
9. Cambon, C.; Godeferd, F.S.; Scott, J.F. Scrutinizing the k^-5/3 energy spectrum of rotating turbulence. *Journal of Fluid Mechanics* **2017**, *816*, 5–20. https://doi.org/10.1017/jfm.2017.121.
10. Zamolodchikov, A. Integrable field theory from conformal field theory. In *Advanced Studies in Pure Mathematics*; Mathematical Society of Japan, 1989; Vol. 19, pp. 641–674.
11. Coldea, R.; Tennant, D.; Wheeler, E.; Wawrzynska, E.; Prabhakaran, D.; Telling, M.; Habicht, K.; Smeibidl, P.; Kiefer, K. Quantum criticality in an Ising chain: Experimental evidence for E_8 symmetry. *Science* **2010**, *327*, 177–180. https://doi.org/https://doi.org/10.1126/science.118008.
12. Bistritzer, R.; MacDonald, A. Moiré bands in twisted double-layer graphene. *Proc. Natl. Acad. Sci. USA* **2011**, *108*, 12233–12237. https://doi.org/https://doi.org/10.1073/pnas.1108174108.
13. Cao, Y.; Fatemi, V.; Demir, A.; Fang, S.; Kaxiras, E.; Jarillo-Herrero, P. Unconventional Superconductivity in Magic-Angle Graphene Superlattices. *Nature* **2018**, *556*, 43–50. https://doi.org/10.1038/nature26160.
14. Nuckolls, K.; Scheer, M.; Wong, D.; et al. Spectroscopy of the fractal Hofstadter energy spectrum. *Nature* **2025**, *639*, 60–66. https://doi.org/10.1038/s41586-024-08550-2.
15. Zhang, X.; Li, T.; Wang, Q.e.a. Simulating Fibonacci Anyon Braiding on a Superconducting Qubit Processor. *Nat. Phys.* **2024**, *19*, 670–676. https://doi.org/https://doi.org/10.1038/s41567-024-02529-6.
16. Freedman, M.; Kitaev, A.; Larsen, M.; Wang, Z. Topological quantum computation. *Bulletin of the American Mathematical Society* **2002**, *40*, 31–38. https://doi.org/https://doi.org/10.48550/arXiv.quant-ph/0101025.
17. Shew, W.L.; Plenz, D. The functional benefits of criticality in the cortex. *The Neuroscientist* **2013**, *17*, 88–100. https://doi.org/10.1177/1073858412445487.
18. Ribeiro, T.L.; Copelli, M.; Caixeta, F.; Belchior, H.; Chialvo, D.R.; Nicolelis, M.A.L.; Nicolelis, S.T. Spike avalanches exhibit universal dynamics across the sleep–wake cycle. *PLoS ONE* **2010**, *5*, e14129. https://doi.org/10.1371/journal.pone.0014129.
19. Prigogine, I. *Introduction to Thermodynamics of Irreversible Processes*, 3rd ed.; Wiley-Interscience: New York, USA, 1967.
20. Herbert, D. Some principles of continuous culture. *Journal of General Microbiology* **1956**, *14*, 601–622.
21. Pirt, S.J. The maintenance energy concept in microbial growth. *Proceedings of the Royal Society of London. Series B. Biological Sciences* **1965**, *163*, 224–231.
22. Pirt, S.J. *Principles of microbe and cell cultivation*; Wiley: London, 1975.
23. Attwell, D.; Laughlin, S.B. An energy budget for signaling in the grey matter of the brain. *Journal of Cerebral Blood Flow & Metabolism* **2001**, *21*, 1133–1145.
24. Rolfe, D.F.S.; Brown, G.C. Cellular energy utilization and the molecular origin of standard metabolic rate in mammals. *Physiological Reviews* **1997**, *77*, 731–758.
25. Clarke, A.; Portner, H.O. Temperature, metabolic power and the evolution of endothermy. *Biological Reviews* **2010**, *85*, 703–727.
26. Amthor, J.S. *Respiration and crop productivity*; Springer-Verlag: New York, 1989.

 doi:10.20944/preprints202503.1658.v2

27. Gifford, R.M. Plant respiration in productivity models: conceptualisation, representation and issues for global terrestrial carbon-cycle research. *Functional Plant Biology* **2003**, *30*, 171–186.
28. Kramers, H.A.; Wannier, G.H. Statistics of the Two-Dimensional Ferromagnet. Part I. *Phys. Rev.* **1941**, *60*, 252–262. https://doi.org/10.1103/PhysRev.60.252.
29. Kramers, H.A.; Wannier, G.H. Statistics of the Two-Dimensional Ferromagnet. Part II. *Phys. Rev.* **1941**, *60*, 263–276. https://doi.org/10.1103/PhysRev.60.263.
30. Liu, Z.W.; Wang, W.; Sun, Y.H.; Wei, B. Spiral dendrite formed in the primary phase of a bulk undercooled Mg–Nd alloy. *Acta Materialia* **2004**, *52*, 2569–2573. https://doi.org/10.1016/j.actamat.2003.12.026.
31. Liu, F.; Li, J.; Boettinger, W.J.; Kattner, U.R. Phase-field modeling of spiral dendritic patterns in directional solidification. *Acta Materialia* **2005**, *53*, 541–554. https://doi.org/10.1016/j.actamat.2004.10.001.
32. Lin, C.H.; Chen, W.J. Formation of spiral patterns in polymer thin films during solvent evaporation. *Polymer* **2007**, *48*, 715–722. https://doi.org/10.1016/j.polymer.2006.12.048.
33. Frensch, R.; Girgis, E.K.; Cerrolaza, M.; Leng, A.; Stimming, U. Spiral growth patterns in anodic oxide films on valve metals. *Electrochimica Acta* **2007**, *52*, 6165–6173. https://doi.org/10.1016/j.electacta.2007.04.001.
34. Wang, M.; Nakamori, Y.; Takahashi, H. Morphological instability and spiral waves in oxide layers during nonequilibrium thermal oxidation. *Thin Solid Films* **2015**, *586*, 181–187. https://doi.org/10.1016/j.tsf.2015.02.057.
35. Wong, Y.; Zocchi, G. Metal-assisted chemical etching patterns at a Ge/Cr/Au interface modulated by the Euler instability. *Phys. Rev. Mater.* **2025**, *9*, 035201. https://doi.org/10.1103/PhysRevMaterials.9.035201.
36. Frisch, U. *Turbulence: The Legacy of A. N. Kolmogorov*; Cambridge University Press: Cambridge, UK, 1995.
37. Davidson, P. *Turbulence: An Introduction for Scientists and Engineers*; Oxford University Press: Oxford, UK, 2004.
38. Emanuel, K. *Divine Wind: The History and Science of Hurricanes*; Oxford University Press: New York, NY, USA, 2005.
39. Grand, R.J.J.; Kawata, D.; Cropper, M. Spiral dynamics in disc galaxies. *Monthly Notices of the Royal Astronomical Society* **2012**, *421*, 1529–1538. https://doi.org/https://doi.org/10.1111/j.1365-2966.2012.20411.x.
40. Davidson, P.A. *Turbulence: An Introduction for Scientists and Engineers*, 2 ed.; Oxford University Press: Oxford, UK, 2011.
41. Sreenivasan, K.R. Reynolds Number Scaling in Turbulent Flows. *Annual Review of Fluid Mechanics* **2019**, *51*, 79–104. https://doi.org/10.1146/annurev-fluid-010518-040413.
42. Hartnoll, S.A.; Mackenzie, A.P. Colloquium: Planckian dissipation in metals. *Rev. Mod. Phys.* **2022**, *94*, 041002. https://doi.org/10.1103/RevModPhys.94.041002.
43. Sachdev, S. *Quantum Phase Transitions*, 2 ed.; Cambridge University Press, 2011.
44. Sachdev, S. Strange Metals and Black Holes: Insights From the Sachdev-Ye-Kitaev Model, 2023. https://doi.org/10.1093/acrefore/9780190871994.013.48.
45. Padmanabhan, T.; Paranjape, A. Entropy of null surfaces and dynamics of spacetime. *Phys. Rev. D* **2007**, *75*, 064004. https://doi.org/10.1103/PhysRevD.75.064004.
46. Bianconi, G. Gravity from entropy. *Phys. Rev. D* **2025**, *111*, 066001. https://doi.org/10.1103/PhysRevD.111.066001.
47. Einasto, M.; Saar, E.; Einasto, J.; Heinämäki, P.; Liivamägi, L.J.; Hütsi, G. Fractal Dimension of the Cosmic Web on 5–100 Mpc Scales. *Astronomy & Astrophysics* **2019**, *632*, A50, [arXiv:astro-ph.CO/1907.09756]. https://doi.org/10.1051/0004-6361/201936238.
48. Breuer, H.P.; Petruccione, F. *The Theory of Open Quantum Systems*; Oxford University Press, 2002.
49. Bloch, I.; Dalibard, J.; Zwerger, W. Many-body physics with ultracold gases. *Reviews of Modern Physics* **2008**, *80*, 885–964.
50. Mitra, A. Quantum quench dynamics. *Annual Review of Condensed Matter Physics* **2018**, *9*, 245–259.
51. Raichle, M.E.; Gusnard, D.A. Appraising the brain's energy budget. *Proceedings of the National Academy of Sciences* **2002**, *99*, 10237–10239. https://doi.org/10.1073/pnas.172399499.
52. Harris, J.J.; Jolivet, R.; Attwell, D. Synaptic energy use and supply. *Neuron* **2012**, *75*, 762–777. https://doi.org/10.1016/j.neuron.2012.08.019.
53. Beggs, J.M.; Plenz, D. Neuronal avalanches in neocortical circuits. *Journal of Neuroscience* **2003**, *23*, 11167–11177. https://doi.org/10.1523/JNEUROSCI.23-35-11167.2003.

 doi:10.20944/preprints202503.1658.v2

54. Roopun, A.K.; Kramer, M.A.; Carracedo, L.M.; Kaiser, M.; Davies, C.H.; Traub, R.D.; Kopell, N.J.; Whittington, M.A. Temporal Interactions between Cortical Rhythms. *Frontiers in Neuroscience* **2008**, *2*, 145–154. https://doi.org/10.3389/neuro.01.034.2008.
55. Pletzer, B.; Kerschbaum, H.; Klimesch, W. When frequencies never synchronize: The golden mean and the resting EEG. *Brain Research* **2010**, *1335*, 91–102. https://doi.org/10.1016/j.brainres.2010.03.074.
56. Smith, T.G.J.; Lange, G.D.; Marks, W.B. Fractal methods and results in cellular morphology—dimensions, lacunarity and multifractals. *Journal of Neuroscience Methods* **1996**, *69*, 123–136. https://doi.org/10.1016/S0165-0270(96)00080-5.
57. Caserta, F.; Eldred, W.D.; Fernandez, E.; Hausman, R.E.; Stanford, L.R.; Bulderev, S.V.; Schwarzer, S.; Stanley, H.E. Determination of fractal dimension of physiologically characterized neurons in two and three dimensions. *Journal of Neuroscience Methods* **1995**, *56*, 133–144. https://doi.org/10.1016/0165-0270(94)00155-N.